Preparation of mesoporous alumina electro-generated by electrocoagulation in NaCl electrolyte and application in fluoride removal with consistent regenerations

A. Oulebsir, T. Chaabane, S. Zaidi, K. Omine, V. Alonzo, A. Darchen, T.A.M. Msagati, V. Sivasankar

Arabian Journal of Chemistry (2020) 13, 271–289

King Saud University

Arabian Journal of Chemistry

www.ksu.edu.sa
www.sciencedirect.com

ORIGINAL ARTICLE

Preparation of mesoporous alumina electro-generated by electrocoagulation in NaCl electrolyte and application in fluoride removal with consistent regenerations

A. Oulebsir [a], T. Chaabane [a], S. Zaidi [a], K. Omine [b], V. Alonzo [c], A. Darchen [c], T.A.M. Msagati [d], V. Sivasankar [b,*]

[a] *Faculty of Mechanical and Process Engineering (FGMGP)/Environmental Department, University of Science and Technology Houari Boumédiène (USTHB), P 32 El-Alia 16111, Bab Ezzouar, Algiers, Algeria*
[b] *Department of Civil Engineering, School of Engineering, Nagasaki University, Nagasaki-Daigaku, 1-14 Bunkyo-machi, Nagasaki 852 8521, Japan*
[c] *UMR CNRS n°6226, Institut des Sciences Chimiques de Rennes, ENSCR, 11 Allée de Beaulieu, CS 50837, 35708 Rennes Cedex 7, France*
[d] *University of South Africa, College of Science Engineering and Technology, UNISA Science Campus, 1709 Roodepoort, Johannesburg, South Africa*

Received 6 January 2017; accepted 3 April 2017
Available online 5 May 2017

KEYWORDS

Electro-generated mesoporous alumina;
Electrocoagulation;
Fluoride removal;
Regeneration;
Model validations;
JMP model

Abstract The fluoride adsorption by Electro-Generated Adsorbents (EGA) was briefly and recently shown. In this paper, the preparation of a particular EGA and its characteristics are presented. For the first time, the fluoride adsorption of one EGA was deeply investigated showing that the regeneration of this material leads to an efficient process which was better than an electrocoagulation one. The investigated adsorbent called EGA_{NaCl} was prepared by electrolysis in NaCl electrolyte with aluminum electrodes and was characterized by X-ray Diffraction (XRD), scanning electron microscopy (SEM) with energy dispersive spectroscopy (EDS), FTIR and BET studies. The physical analyses showed that EGA_{NaCl} was a mesoporous mixture of AlOOH and three Al $(OH)_3$ which contain the chlorine element and registered the surface area of 114.31 $m^2 g^{-1}$. The presence of chlorine explains the pH increase observed during the electrolysis. The fluoride adsorption as a function of pH, initial fluoride concentration, EGA_{NaCl} dose, temperature, co-ions and cycles of regeneration was studied using batch methods. Among the kinetic models, the pseudo –

* Corresponding author at: Post Graduate and Research Department of Chemistry, Pachaiyappa's College, Chennai, Tamil Nadu 600 030, India.
E-mail address: sivshri.20@gmail.com (V. Sivasankar).
Peer review under responsibility of King Saud University.

Production and hosting by Elsevier

http://dx.doi.org/10.1016/j.arabjc.2017.04.007

second – order model was superior to others and among the adsorption isotherms, Langmuir model fits well as compared to that of Freundlich model based on the regression coefficient values. Determination of thermodynamic parameters such as ΔH and ΔG respectively revealed the nature of endothermic and temperature – driven nature of the fluoride sorption process. The maximum adsorption capacity of EGA_{NaCl} was found to be 16.33 mg g^{-1} at 27 °C and a maximum fluoride removal occurred at pH 6.55. The spent adsorbent showed the defluoridation efficiency of 95.53% up to fifth regeneration with diluted NaOH. Factorial design matrix and analysis of variance using JMP model have also been extensively discussed in this paper.

1. Introduction

Fluoride contamination of drinking water is well known in many countries where it leads to many diseases. This situation induces a lot of researches which aim to improve the fluoride abatement (Sivasankar, 2016). Many methods have been investigated in the defluoridation of drinking water (Darchen et al., 2016). Among these methods, the adsorption onto adsorbents which contains fluorophilic elements appears as the best method and aluminum is one of the most investigated fluorophilic elements. Many researches about defluoridation are conducted in two directions: (i) the preparation of new aluminas, and (ii) the development of electrocoagulation, which may be seen as a specific synthesis for aluminum adsorbent from a soluble aluminum anode. Adsorption onto alumina and electrocoagulation (Guzman et al., 2016) are the main operations in industrial and domestic defluoridations (Darchen et al., 2016). For the moment, alumina is the main adsorbent used in industrial defluoridation plants (Schoeman, 2009) and recommended by the US Environmental Protection Agency EPA as a defluoridation adsorbent of drinking water (US EPA, 2003). Despite this uses, many works were recently devoted to the research of new aluminas (Saleh and Gupta, 2012) and their activities in defluoridation (Patankar et al., 2013; Teutli-Sequeira et al., 2012; Jimenez-Becerril et al., 2012; Wu et al., 2016).

Activated alumina was investigated in domestic defluoridation units (Chauhan et al., 2007) or in column (Ghorai and Pant, 2004). The effect of pH on fluoride adsorption (Ku and Chiou, 2002) and the content of aluminum in defluoridated water were studied (George et al., 2010). Five aluminas were synthesized at different pH and calcination temperatures and their fluoride adsorption activities were investigated (Gong et al., 2012). Defluoridation by adsorption process using adsorbents such as acidic alumina (Goswami and Purkait, 2012), aluminum hydroxide (Shimelis et al., 2006), boehmite AlOOH (Liu et al., 2011) and freshly prepared aluminum hydroxides (Liu et al., 2011) has been reported. Different kinds of composite materials which contain aluminum hydroxide or alumina were also investigated in fluoride adsorption: aluminum hydroxide coated rice hush ash (Ganvir and Das, 2011), mixed alumina-magnesia hydroxide adsorbent (Patankar et al., 2013), alumina cement granules (Ayoob et al., 2008; Ayoob and Gupta, 2009) and magnesia-amended alumina granules (Maliyekkal et al., 2008). Various kinds of nanomaterials were also synthesized and investigated in defluoridation such as adsorption by nano-alumina (Kumar et al., 2011), aluminum oxide hydroxide (Wang et al., 2009a,b), nanoparticles of gamma alumina (Singh et al., 2016) and alumina nanoparticles synthesized by flame spray pyrolysis method (Tangsir et al., 2016). According to our literature survey, only a very few reports on the use of electrogenerated aluminas has been published (Netpradit et al., 2004; Santos et al., 2008; Zidane et al., 2008; Golder et al., 2006a, 2006b; Garcia-Gomez et al., 2016). Most of them used sludge waste generated in electrocoagulation treatment (Netpradit et al., 2004; Santos et al., 2008; Zidane et al., 2008; Golder et al., 2006a, 2006b) for dye adsorption (Netpradit et al., 2004; Santos et al., 2008; Zidane et al., 2008; Golder et al., 2006a) and phosphate removal (Golder et al., 2006b).

There are only few papers about the electrochemical preparation of adsorbents under controlled conditions and their uses in adsorption treatments (Garcia-Gomez et al., 2016; Flilissa et al., 2016; Tchomgui-Kamga et al., 2013; Zaidi et al., 2016). Garcia-Gomez et al. (2016) synthesized the electrocoagulated metal hydroxide (EMHS) using aluminum electrodes as an adsorbent for the removal of fluoride and arsenic ions. Flilissa et al. (2016) attempted on the removal of cetylpyridinium ion using the electrogenerated aluminum phosphate. Few Electro-Generated Adsorbents (EGAs) have been recently investigated as adsorbents in the removal of doxycycline from aqueous solutions (Zaidi et al., 2016). EGAs constitute a new class of adsorbents which can be prepared in soft and controlled conditions and their efficiency merits to be investigated. In the research of new aluminas for defluoridation, the preparation of EGAs has been described by electrolysis with aluminum electrodes in electrolyte containing monovalent cations (Tchomgui-Kamga et al., 2013). This work showed the effect of the electrolyte on the structure of the EGAs and the defluoridation activity of the prepared EGAs was briefly evaluated in a 10 mg/L of fluoride solution showing fluoride abatement in the range 57–99%. The present paper intends to prove the interest of these materials by investigating one particular EGA toward the fluoride adsorption. This adsorbent EGA_{NaCl} was prepared by electrolysis using aluminum electrodes and NaCl electrolyte. It was selected for the present study because it was one of the best EGAs in defluoridation (Tchomgui-Kamga et al., 2013), despite its mixed structure. In the present work, for the first time, the defluoridation efficiency was deeply investigated which includes the regeneration of the exhausted adsorbent in order to show that adsorption process with multiple regenerations is more efficient than an electrocoagulation process.

2. Materials and methods

2.1. Chemicals

All the chemicals used in both the electrochemical and the adsorption processes were of analytical grade and purchased from Sigma-Aldrich (France and India). All the solutions were prepared using double distilled water. Aluminum used for electrodes was 1050 Å of the registered international designation purchased from Ridings and Dafrodis (Bouc-Bel-Air, France).

2.2. Electro-synthesis of EGA_{NaCl}

Electrolyses were carried out in a reactor of 1.5 L of capacity with magnetic stirring. The electrolyte was 1 L of an aqueous solution of 0.1 M NaCl. Electrodes were aluminum plates of 11.5 cm × 4.7 cm × 0.4 cm dimensions. The gap between the electrodes was of 1 cm. Electrodes were connected to a digital DC supply (2303 GPS-type) with voltage and current range of 0–32 V and 0–4 Å, respectively. A digital ammeter and volt-

meter were used to measure the current or the voltage. Before electrolysis, the aluminum electrodes were immersed in 0.1 M NaOH for 10 min. Then these electrodes were rinsed with distilled water and dried at 105 °C for 10 min. A typical electrolysis is as follows. Freshly prepared electrodes were weighed, then immersed in the electrolyte and finally connected to the DC supply. The electrolyses were performed with a constant current. The solution was magnetically stirred. At regular intervals, samples of solution were taken to carry out measurements of pH, turbidity, and conductivity with an electronic pH-meter (Metrohm), a turbidimeter (Hach) and a conductivity meter (Radiometer Meterlab CDM 210), respectively. The electrolysis course was investigated with a current of 0.3 or 0.7 Å. The preparation of EGA_{NaCl} for the fluoride removal studies was performed with a current of 0.7 Å for 2 h. At the end of the electrolyses, the electrogenerated solid was collected by filtration and then rinsed three times with distilled water under agitation and finally dried in an oven at 105 °C for 24 h. About 1.9 g of dried material was obtained. The used electrodes were rinsed with distilled water and then dried at 105 °C for one hour and finally weighed.

2.3. Instrumental characterization

The samples were analyzed by X-ray powder diffraction (XRD) using a PANalytical Empyrean diffractometer (θ–θ Bragg–Brentano geometry) working with the Cu Kα radiation ($\lambda\ K\alpha_1$ = 1.5406 Å, $\lambda\ K\alpha_2$ = 1.5444 Å). Data were collected with a PIXcel1D detector, in the angular range 5–80° (2θ). Match! software (Cristal Impact, Germany) was used to display XRD diagrams and to identify phases by comparison with reference database. The infrared spectra were recorded using a Thermo Scientific Nicolet iS5 FT-IR spectrometer with iD7 ATR accessory. A small amount of the ground sample was laid down on the diamond crystal. Infrared spectra were recorded from 4000 to 400 cm^{-1}. Omnic software was used to display spectra. Observations with a Scanning Electron Microscope (SEM) and element analysis by Energy Dispersive Spectroscopy (EDS) were performed using Jeol JSM 6400 equipment operating at an accelerating voltage of 20 kV.

The physical and structural characteristics were determined by nitrogen adsorption/desorption at 77.5 K using Micromeritics ASAP 2020 surface area and porosity size analyzer.

2.4. Analytical techniques

Fluoride removal experiments were performed with dilution of a homemade stock solution of 100 mg L^{-1}. The defluoridation experiments were carried out by the batch method at temperatures of 300 K, 313 K and 323 K, various pH values, EGA_{NaCl} doses and fluoride concentrations of 2.78, 4.41 and 5.31 mg L^{-1}. The residual fluoride concentrations were determined with a fluoride ion selective electrode (Orion, number 9609, USA) connected to an ion meter (Orion, model 290A, USA). The fluoride samples were diluted to 1:1 with a commercial buffer (TISAB II, Orion). The specific amount of fluoride adsorbed was calculated from Eq. (1) where Q_e is the adsorption capacity at the equilibrium (mg g^{-1}), C_0 and C_e are respectively the initial and the equilibrium fluoride concentration (mg L^{-1}), V is the volume of the aqueous solution (L) and W is the mass (g) of EGA_{NaCl}.

$$Q_e = \frac{(C_0 - C_e)V}{W} \quad (1)$$

The pH of point of zero charge (pH_{PZC}) was determined by the following method. 100 mg of EGA_{NaCl} was added to 50 mL of 0.05 M $NaNO_3$ deoxygenated aqueous solutions with a pH range of 1–12. Blanks with no adsorbent were also run in the same initial pH values. After magnetically shaking for 24 h at room temperature, the final pH was measured. The pH_{PZC} was determined as the pH of the $NaNO_3$ solution that remained unchanged after contact with EGA_{NaCl}. The isoelectric point (IEP) for EGA_{NaCl} was determined by potentiometric titration with the support of electrophoretic technique using Zetasizer Nano with 633 nm He-Ne laser equipped with an MPT-2 autotitrator (Malvern, U.K). Series of 0.01 M and 0.001 M NaCl solutions (0.1 g per 50 mL) from initial pH 2 – 12 were mechanically agitated for 24 h at room temperature. Later, the above solutions were calculated for ζ potentials using Smoluchowski equation.

The effect of co-existing anions was investigated during defluoridation experiments which were conducted for fluoride concentration of 2.78 mg L^{-1} for an equilibrium time of 35 min at 300 K. The various co-ion solutions of 50, 100 and 200 mg L^{-1} were prepared with sodium salts of chloride, nitrate, hydrogen carbonate, sulfate and phosphate. Regeneration experiments were conducted using 0.05 M NaOH solution with the spent EGA_{NaCl} for the time of 35 min. The sorption of fluoride using the initial fluoride concentration of 2.78 mg L^{-1} at an optimized pH was initially carried out for the optimized equilibrium time and followed by the regeneration study. The adsorption and regeneration cycles were attempted up to six operations. Validation of kinetic and isotherm models was made using the experimental data. The determination of thermodynamic parameters such as ΔG^o, ΔH^o and ΔS^o was also calculated.

2.5. JMP statistical software

The statistical method called Response Surface Methodology (RSM) uses the quantitative results from appropriate experiments for determining regression model equations and suitable operating conditions (Alam et al., 2007). RSM is the incorporation of mathematical and statistical techniques for modeling and analysis of problems where the response of interest is influenced by several variables (Montgomery, 2001).

A standard RSM design called full factorial design (FFD) was applied in this work to study the effect of variables on the adsorption of fluoride from aqueous solution using EGA_{NaCl} in a batch mode experiments. The FFD was widely used for fitting a linear and quadratic model. By using this method, modeling is possible with the requirement of only a minimum number of experiments. It is not necessary in the modeling procedure to know the detailed reaction mechanism since the mathematical model is empirical. Generally, the number of factors under study allowed the choosing of FFD rather than a fractional factorial design that further reduces the number of experiments (Montgomery, 2001), which may decrease the reliability of the model. The fluoride sorption efficiency

onto EGA_{NaCl} made the subject of the study, and was chosen as the model response (Y, mg g^{-1}). The main factors affecting this sorption efficiency are the temperature, EGA_{NaCl} dose and the contact time. For this modeling, all experiments are provided in order to achieve the number m^n FFD model. Each variable is investigated at three levels. Meanwhile, as the number of factors (n) increases, there would be a rapid increase in the number of runs for a complete replicate of the design. In this case, main effects and interactions may be estimated by full factorial designs running by all the experiments suggested by models. The individual second-order effects can be estimated separately by the FFD and only the third-order effect is supposed to be insignificant. The resulting responses and the corresponding parameters are modeled and optimized using ANOVA. Basically this optimization process involves three major steps such as, performing the statistically designed experiments, estimating the coefficients in a mathematical model and, predicting the response and thereby checking the adequacy of the model.

$$Y = f(X_1, X_2, X_3, X_4, \ldots X_n) \tag{2}$$

where Y is the response of the system and Xi is the variables of action called factors. The goal is to optimize the response variable (Y), which is the maximization goal. It is assumed that the independent variables are continuous and controllable by experiments with negligible errors. It is required to find a suitable approximation for the true functional relationship between independent variables and the response surface (Gunaraj and Murugan, 1999). The experimental sequence was randomized in order to minimize the effects of the uncontrolled factors. The response was used to develop an empirical model by the correlation of the response with the fluoride sorption from the aqueous solution using EGA_{NaCl} with the help of two different polynomial (quadratic and linear) Eqs. (3) and (4) as follows:

$$Y = b_0 + \sum_{i=1}^{n} b_i X_i + \sum_{i=1}^{n} b_{ii} X_i^2 + \sum_{i=1}^{n} \sum_{j>1}^{n} b_{ij} X_i X_j \tag{3}$$

$$Y = b_0 + \sum_{i=1}^{n} b_i X_i + \sum_{i=1}^{n} \sum_{j>1}^{n} b_{ij} X_i X_j + \sum_{i=1}^{n} \sum_{j>1}^{n} \sum_{k>2}^{n} b_{ijk} X_i X_j X_k \tag{4}$$

In the above equations, Y is the predicted response, b_o the constant coefficient, bi the linear coefficients, bij the interaction coefficients, bii the quadratic coefficients and xi, xj are the coded values of the adsorption of fluoride onto EGA_{NaCl} variables. The central points are chosen such that they allow readability, which ensures that the variance of the model prediction is constant at all points equidistant from the design center (Box and Hunter, 1975). The number of experiments (N) is defined by the choice of the number of factors and their levels. In the case of a three – level study with three factors, the number of experiments is equal to N (equal to 3^3). Thus the number of experience allowed to study all the probabilities and possible configurations between the three factors and three levels. Hence, the total number of tests (N) required for the three independent variables (m) at the three levels (n) is 27 ($N = 3^3$).

3. Results and discussion

3.1. Preparation of EGA_{NaCl}

The electrolyses were carried out at room temperature in 0.1 M NaCl solution. The electrolysis current was controlled at 0.7 A. After 120 min of electrolysis the mass loss of the anode was 0.565 g, it was larger than the mass loss calculated at 0.469 g by using the Faraday law. The cathode showed also a mass loss of 0.182 g. These mass losses for both electrodes are usual observations in electrolysis with aluminum electrodes. The larger mass losses are due to concomitant corrosion which contributes to the formation of 1.936 g of the electrolysis products.

Owing to the formation of EGA_{NaCl}, the turbidity of the solution nearly increased linearly as shown in Fig. 1A. At the end of electrolysis, the turbidities are proportional to the current. This observation and the linear increase may be explained by the formation of homogeneous particles.

At the beginning of electrolysis, the pH increased and reached an approximate constant value as shown in Fig. 1B. The pH increase was larger for larger current. This increase in pH was explained by the involvement of chloride anion in competition with hydroxide anion leading to incorporation of chloride into the aluminum hydroxides (Eqs. (5) and (6)) while the released hydroxide anion increases the pH (Tchomgui-Kamga et al., 2013).

$$AlOOH + Cl^- \rightarrow AlOCl + OH^- \tag{5}$$

$$Al(OH)_3 + Cl^- \rightarrow Al(OH)_2Cl + OH^- \tag{6}$$

In agreement with the pH increase, concomitant increase in the conductivity was observed as shown in Fig. 1C. These conductivity increases can be attributed to the electrical mobility of hydroxide anion which is larger than the one of chloride anion.

3.2. Characterization of EGA_{NaCl}

The SEM images of EGA_{NaCl} are presented in Fig. 2(A)–(C). Despite the mixture of crystallized aluminum compounds in EGA_{NaCl}, SEM images show almost homogenous particles which are planar particles of about 0.1–1 μm. This structure offers large surface area for the access of fluoride anions. The EDS results showed that Al and O were the main elements detected. Besides these elements, Cl was also detected at about 2 atomic%. The absence of Na, or its very low concentration, is in agreement with the occurrence of the exchange reactions of Eqs. (5) and (6) which explain the increase in pH during the electrolysis (Tchomgui-Kamga et al., 2013).

The XRD patterns of EGA_{NaCl} powder are presented in Fig. 3A and B. There are a lot of peaks in which it is possible to identify the presence of aluminum oxide hydroxide or boehmite AlOOH, characterized by small broad peaks at 2θ = 14.5° and 28.3° for the most noticeable ones. The other peaks correspond to three aluminum hydroxides $Al(OH)_3$. The enlargement of the angular scale of the diffractogram (Fig. 3B) shows the presence of gibbsite, bayerite and nordstrandite. This composition of EGA_{NaCl} is confirmed by the IR spectrum (Fig. 4) which exhibits distinct bands in the 3000–3700 cm^{-1} range, assigned to the stretching vibration

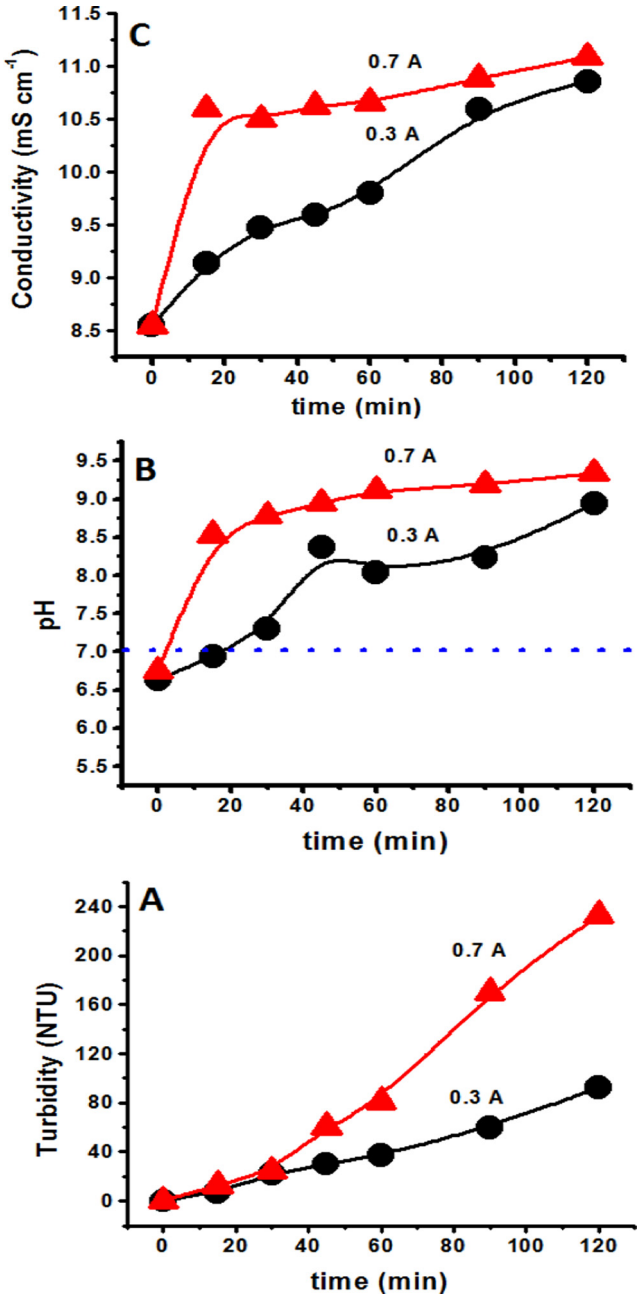

Fig. 1 Influence of current on turbidity (A), pH (B) and conductivity (C) during electro-generation of EGA_{NaCl}. *Conditions:* Volume of NaCl – 1 L; Concentration of NaCl – 0.1 M; Temperature – 300 K; Time – 120 min; Anode and Cathode – Aluminium.

of O—H bonds of the different polymorphs of aluminum hydroxides and also of the boehmite (Elderfield and Hem, 1973; Music et al., 1998; Ogorodova et al., 2012). It is remarkable that four crystallized aluminum compounds are obtained in the same electrolysis. Their formation cannot be explained by three origins of aluminum: the corrosion of the anode and the cathode and the anodic dissolution of the anode.

The nitrogen adsorption-desorption analysis for EGA_{NaCl} and the textural properties based data are shown in Table 3. According to IUPAC classification (Betiha et al., 2011), the EGA_{NaCl} material shows Type IV isotherms characteristic of H4 type (Fig. 5A) with the desorption branch leading to the lower closure point at P/P_o is equal to 0.46. In general, this relative pressure is inferred to be almost independent of the nature of the porous EGA_{NaCl} but depends mainly on the adsorptive (Betiha et al., 2011). The Type H4 loop is not supposed to exhibit any limiting adsorption at high P/P_o with aggregates organized as an assemblage of particles which tend to be loosely coherent. These EGA_{NaCl} aggregates are recognized to resemble plate – like particles giving rise to slit – like pores (Sing et al., 1985). The isotherm hysteresis demonstrates that a pronounced condensation step in the relative pressure range (P/P_o) 0.1–0.2 suggests the narrow – sized mesoporous materials (Benítez-Guerrero et al., 2014). The following second condensation of nitrogen associating the nitrogen uptake at the relative pressure (P/P_o) greater than 0.8 indicates the possible isothermal sorption due to large voids between EGA_{NaCl} particles. The distribution of pore size of EGA_{NaCl} is illustrated in Fig. 5B. It shows a narrow curve in the range of ca. 1.6–2.4 nm with the maximum pore volume of 0.015 $cm^3\ g^{-1}$. This is followed by another gradation between 2.5 nm and 7.0 nm with pore volume of 0.0075 $cm^3\ g^{-1}$. Then the gradation in pore volume reaches 0.0125 $cm^3\ g^{-1}$ and thereafter a declination was observed up to 40 nm. The average pore diameter was observed to be 6.64 nm. The recorded BET surface area of 114.31 $m^2\ g^{-1}$ for the crystalline phases contained EGA_{NaCl} is close to that of the amorphous *in – situ* $Al_2O_3{\cdot}xH_2O$ (118.24 $m^2\ g^{-1}$) with low crystalline nature (Liu et al., 2011). Fang et al., 2016 reported the surface area (111.65 $m^2\ g^{-1}$) for the calcined $Al(OH)_3$ of amorphous type was increased about 100 times to that of raw $Al(OH)_3$. The enrichment of surface area was achievable when the process was maintained at 500 °C for 240 h. But 50% of the time was required for the preparation of EGA_{NaCl} in different crystalline phases by this electro-synthesis. The textural properties of EGA_{NaCl} are represented in Table 3.

3.3. Fluoride adsorption studies

3.3.1. Influence of pH

The parameter which influences the sorption of fluoride at the water – sorbent interfaces is significantly pH and is associated with pH_{zpc} (Jin et al., 2015). Fluoride sorption onto alumina is strictly governed by pH and particularly at weakly acidic pH levels (Ku and Chiou, 2002). Either low or high pH conditions are favorable for the dissolution of Al species. Based on theories, solutions with pH < 5.5, Al^{3+} ions appear whereas pH > 8 aluminates are formed.

Solution pH could affect the surface properties of EGA_{NaCl} and hence the protonation – deprotonation degree of oxygen – containing functional groups directly (Zou et al., 2016).

The trend of pH versus adsorbed fluoride (Fig. 6A) begins from pH 2 with the low fluoride uptake amount of 8.95 mg g^{-1} (24.1% of fluoride removal). Later, the plot gradually elevates and reaches a maximum fluoride uptake of 16.33 mg g^{-1} at pH 6.55. Then the curve continued with a descending trend toward the low fluoride uptake amount of 5.20 mg g^{-1} at pH 11.5. The pH value of 6.55 less than pH_{zpc} of 6.7 (Fig. 7A) favors a positively charged nature due to excess H^+ on the EGA_{NaCl} surface which facilitates the coulombic attractive force with the fluoride ions (Eqs. (7) and (8))

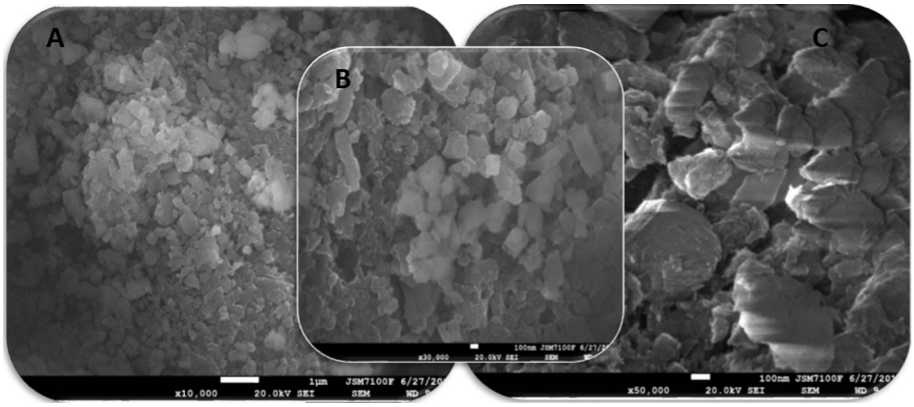

Fig. 2 Scanning electron micrographs with EDAX for EGA_{NaCl} at different magnifications (A, B and C).

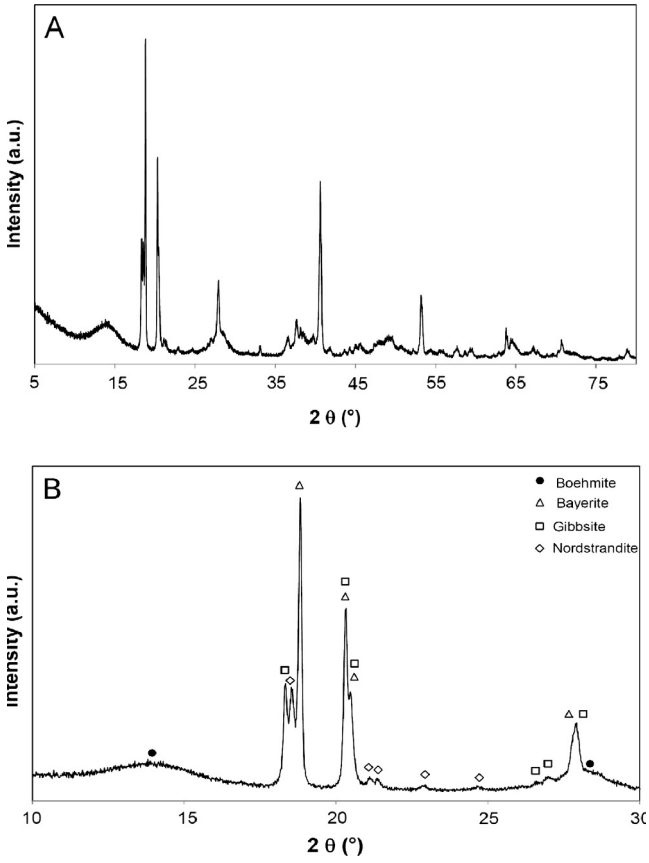

Fig. 3 X-ray diffraction pattern of EGA_{NaCl} (A) Expanded pattern of 2θ between 10 and 30 (B).

$$EGA \equiv OH + H^+ \rightleftarrows EGA \equiv OH_2^+ \quad (7)$$

$$EGA \equiv OH_2^+ + H^+ \leftrightarrow EGA \equiv OH_2^+ \ldots F^- \quad (8)$$

where $\equiv OH_2^+$ is the positive hydroxo group on the surface of EGA_{NaCl}.

It was reported (Hao and Huang, 1986) that, at pH greater than 7, the sorption of fluoride onto EGA_{NaCl} takes place through a ligand exchange mechanism as Eq. (9),

$$EGA \equiv OH + F^- \rightleftharpoons EGA \equiv F + OH^- \quad (9)$$

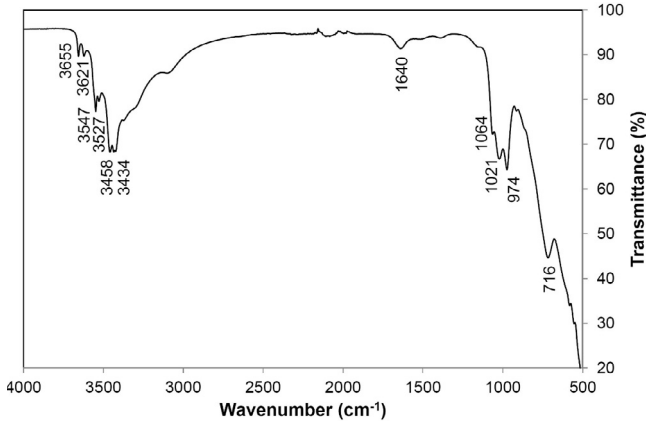

Fig. 4 FTIR spectrum of EGA_{NaCl}.

Fig. 7B shows the plot of pH versus zeta potential (mV) for EGA_{NaCl} which determines the Isoelectric point (IEP) for EGA_{NaCl}. It is a point at which the electrophoretic mobility is zero or a reverse sign representation of zeta potential. Assumption of aged alumina surface coated by amorphous $Al(OH)_3$ can be substantiated from zeta potential measurements and solid – solution equilibria. From the measurements, the values of IEP were determined to be 7.4 and 7.6 respectively for 0.01 M and 0.001 M NaCl solutions respectively. The zeta potential values decreased with the increasing pH values. The electrophoresis measurements showed the IEP shift toward lower pH due to the significant adsorption of background NaCl electrolyte. Consequently, the positively charged EGA_{NaCl} surface gets neutralized with the anions of the electrolyte and causes the decrease in the IEP. The development of significant positive charges at pH 3.0–6.5 indicates the high sorption efficiency of EGA_{NaCl} toward negatively charged fluoride ions and further suggested that the governing mechanism may be electrostatic in nature.

In the case of EGA_{NaCl}, pH greater than 6.55 followed a gradual declination up to pH 10 with 10.08 mg g^{-1} (27.2% of fluoride removal) of fluoride uptake and then a sudden fall at pH 11.5 with the removal of 14.3%. At high pH values, exceeding the pH 11.5, the gradual distortion of hydroxo groups leads to form a surface with increasing negative charge. In addition, the OH^- ions compete against fluoride for the

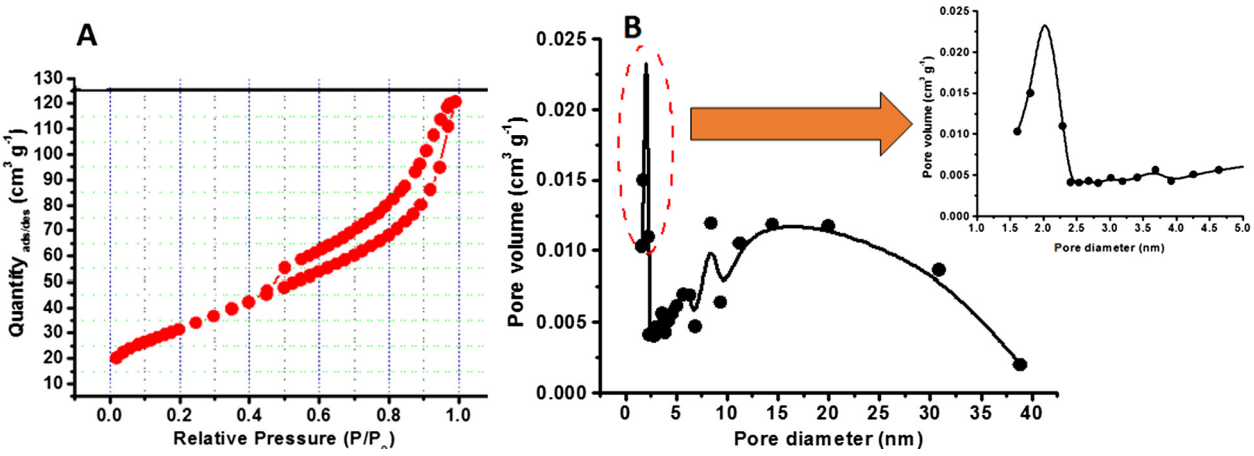

Fig. 5 Nitrogen adsorption – desorption isotherm of EGA_{NaCl} (A) Pore size distribution of EGA_{NaCl} (B).

active sites and the electrostatic repulsion caused between negatively charged fluoride and the EGA_{NaCl} surface. Due to the above facts, fluoride removal at high pH was studied with appreciable reduction. The lower fluoride removal capacity at acidic pH levels may be attributed to the HF ion formation (Raichur and Basu, 2001) or complexation of fluoride ions with dissolved aluminum. The decreasing sorption of fluoride below pH 5 can also be associated with alumina dissolution promoted by fluoride (Nordin et al., 1999) and made clear by Reyes Bahena et al. through the solubility – pH diagram of α-Al_2O_3. In addition, the fluoride enhanced solubility of aluminum hydro(oxides) is possible at low pH conditions due to the formation of predominant aluminum – fluoro complexes (AlF_2^+, AlF^{2+}, AlF_3(aq), and AlF_4^-) in solution. In support of the present study, several researchers explored the optimal pH level between pH 6 and pH 7 and obtained the maximum defluoridation efficiency (Gong et al., 2012; Kumar et al., 2011; Yang et al., 2014; Zhang and Jia, 2016; Tripathy et al., 2006; Du et al., 2014; Wang et al., 2009a,b).

3.3.2. *Influence of EGA_{NaCl} dose*

EGA_{NaCl} dose optimization strategy was adopted using 2.78 mg L^{-1} of fluoride solution at an optimized pH of 6.55 for 35 min of equilibrium time. The plot of EGA_{NaCl} dose versus adsorbed fluoride (Fig. 6B) depicted an increase in fluoride uptake, initially up to 0.075 g and later descends till the EGA_{NaCl} dose was 0.25 g. After this, there was a meagre decrease observed and reaches almost a constant value. The initially increased EGA_{NaCl} was able to adsorb more fluoride with 2.31 mg of difference and can be pertinent to the availability of more active sites on the surface. But a declination was observed after the dose amount of 0.075 g till 0.25 g of EGA_{NaCl}. This could be associated with the superfluity of higher doses for the sorption of limited quantity of fluoride. The operation of negligible driving forces for fluoride sorption at higher doses may also be corroborated. The attainment of constancy in fluoride sorption after 0.25 g of EGA_{NaCl} may be associated with the overlapping of active sites and decrease in the surface area due to the conglomeration of exchanger particles (Killedar and Bhargava, 1993). A factor which reflects the binding ability of an adsorbent is called distribution coefficient, K_D (Murray and Stumm, 1988). It depends on the adsorbent's surface and pH of the solution and is calculated from Eq. (10),

$$K_D = \frac{Cs}{Cw}\ (\mathrm{L\ kg^{-1}}) \tag{10}$$

where C_s is the concentration of fluoride on the solid particles (mg kg^{-1}) and C_w is the equilibrium concentration in solution (mg L^{-1}). The increasing K_D value with respect to EGA_{NaCl} dose reflects the surface heterogeneity of EGA_{NaCl} as evidenced by early researchers using different aluminum oxide adsorbents (Gong et al., 2012; Tripathy et al., 2006).

3.3.3. *Influence of initial fluoride concentration, $[F]_o$*

The influence of initial fluoride concentrations in the defluoridation potential of EGA_{NaCl} was conducted at an optimal pH (6.55), EGA_{NaCl} dose (0.075 g) and temperatures (300 K, 313 K and 323 K). The trend of fluoride sorption as a function of initial fluoride concentration and temperature is shown in Fig. 6C. It is quite evident that the fluoride uptake by EGA_{NaCl} is directly proportional to both initial concentrations and temperature. The fluoride removal as a function of temperature increased from 300 K to 323 K. The observed range of fluoride removal was 44.1–64.1%, 50.8–95.1% and 74.9–85.9% at 300 K, 313 K and 323 K respectively for the chosen range of initial fluoride concentration. Temperature is one of the factors which can affect the surface charge and pH_{zpc} of alumina (Reyes Bahena et al., 2002). Even a small change in temperature could have a strong influence in fluoride sorption toward the formation of stable complexes. The influence of initial fluoride concentration at a particular temperature demonstrates the possibility of fluoride sorption not only onto $EGA \equiv OH_2^+$ but also on the electrically uncharged $Al \equiv OH$ sites as surface exchange reactions (Eqs. (8) and (9)). It may be justified such that the saturated sorption sites on the surface of EGA_{NaCl} may not be prioritized for further sorption. The factual reason is that the mutually proportional factors such as concentration gradient and adsorption rate depend on the adsorption sites of EGA_{NaCl}.

3.3.4. *Inhibition by interfering ions*

The purpose of this study is to explore the inhibition to fluoride sorption onto EGA_{NaCl} by other interfering ions such as

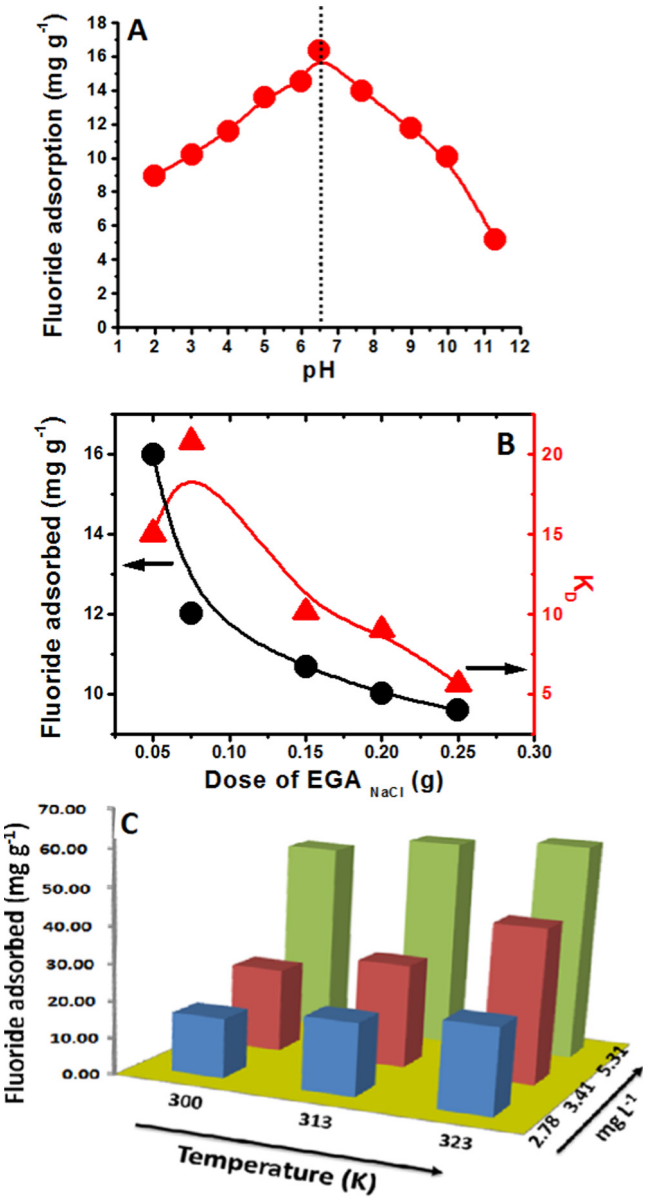

Fig. 6 pH influence (A) dose influence (B) temperature $[F]_o$ influence in mg L^{-1} (C) for the fluoride sorption onto EGA_{NaCl} *Conditions:* (A) EGA dose – 0.1 g; Time – 35 min; $[F]_0$ – 2.78 mg L^{-1}; T – 300 K. (B) pH – 6.55; Time – 35 min; $[F]_0$ – 2.78 mg L^{-1}; T – 300 K. (C) pH – 6.55; Time – 35 min; EGA dose – 0.1 g.

chloride, nitrate, phosphate, sulfate and hydrogen carbonate as these major anions are present in groundwater. Among the interfering anions, hydrogen carbonate was the most inhibiting and chloride was the least inhibiting anions. The inhibition percentage increased with the increase in the concentration of anions (50–200 mg L^{-1}) as shown in Fig. 8A. The maximum negative interference by chloride, nitrate, sulfate, phosphate and hydrogen carbonate was recorded as 15.6%, 17.9%, 38.2%, 43.0% and 77.0% respectively for the anionic concentration of 200 mg L^{-1}. Among the interfering ions, the highest inhibition due to hydrogen carbonate was associated with the raise in the pH level (8.5–11.0) toward basic condition and the competency for the same sorption site as well. The maximum inhibition due to hydrogen carbonate for fluoride sorption using aluminum adsorbents has already been reported by early researchers (Patankar et al., 2013; Nigussie et al., 2007; Kamble et al., 2010). The interference of phosphate to fluoride sorption may be associated with the enabled formation of aluminum phosphate under alkaline conditions as phosphates have strong affinity over aluminum (III) species (Ayoob and Gupta, 2009). The inhibitory action of sulfate may be envisaged due to the formation of partial outer and inner sphere complex formation and its divalent nature repulsion against fluoride (Sujana et al., 1998). The interference patterns of chloride and nitrate (low affinity ligands) indicated the formation of weaker bonds with the active sites on the EGA_{NaCl}'s surface through outer sphere mechanism. Hence lower inhibitory influence on fluoride sorption was observed due to chloride and nitrate ions.

3.4. Kinetic and isotherm models

Table 1 shows the kinetic and isotherm data for the fluoride sorption onto EGA $_{NaCl}$ controlled at different temperatures (300 K, 313 K and 323 K) and initial fluoride concentrations (2.78 mg L^{-1}, 3.41 mg L^{-1} and 5.31 mg L^{-1}).

The fluoride kinetics based on pseudo – order – model is validated using the linearized – integral form (Lagergren, 1898) to describe adsorption in solid – liquid systems, where the adsorption depends on the solid capacity (Ho, 2004). The pseudo – first – order rate constant (k_1, min^{-1}) and q_e (mg g^{-1}) are calculated from the slope and the intercept of Eq. (11) respectively.

$$\ln(q_e - q) = \ln\left(\frac{k_1}{2.303}\right)t \tag{11}$$

where q_e and q are the adsorption capacities at equilibrium and a particular time (min) respectively. The pseudo – first – order rate constant for the chosen fluoride concentrations was in the range of 0.090–0.112 min^{-1}, 0.082–0.085 min^{-1} and 0.065–0.101 min^{-1} respectively for 300 K, 313 K and 323 K.

The pseudo – second – order model (Ho, 2006) can be expressed by the following Eq. (12) and is based on the assumption that the rate-limiting step may be chemical sorption or chemisorption involving valence forces through sharing or exchanging electrons between the sorbent and sorbate.

$$\frac{t}{q_t} = \frac{1}{k_2 q_{e^2}} + \frac{1}{q_e}t \tag{12}$$

Fig. 9(A)–(C) shows the plot of t/q_t versus t and from which the pseudo – second – order rate constant (k_2, g mg^{-1} min^{-1}), initial sorption rate (h, mg g^{-1} min^{-1}) and equilibrium sorption capacity (q_e, mg g^{-1}) can be determined. It is apparent that the second – order equilibrium sorption capacity (q_e) increased with respect to initial fluoride concentration and temperature. The kinetic data of pseudo – second – order model revealed that the influence of initial fluoride concentration doubled the q_e values (2.2 times at 300 K and 2.1 times at 313 K) from 3.41 mg L^{-1} to 5.31 mg L^{-1}. At 300 K and 313 K, the influence between the first two concentrations (2.78 mg L^{-1} and 3.41 mg L^{-1}) was lower than between the second and third fluoride concentrations (3.41 mg L^{-1} and 5.31 mg L^{-1}). The influence of fluoride concentration seems to be reversed at

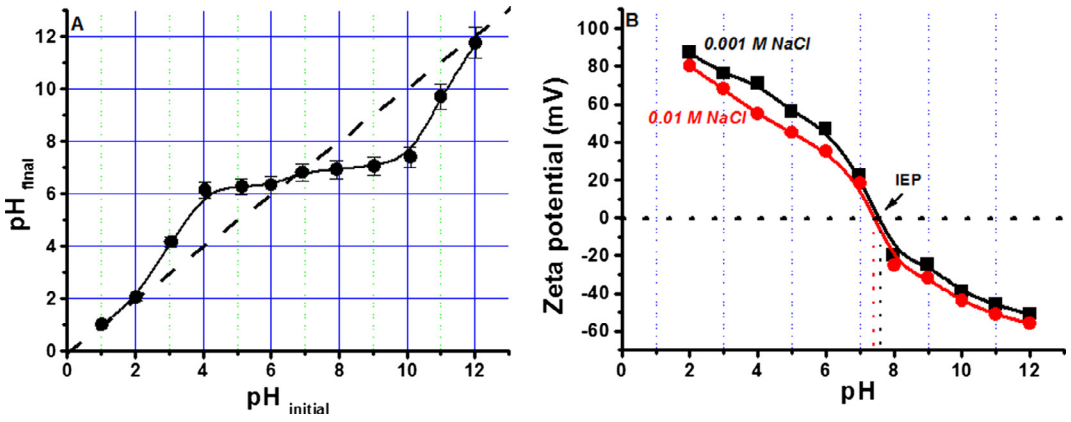

Fig. 7 pH_{zpc} (A), plot of pH versus Zeta potential (B). *Conditions:* (A) EGA dose – 0.1 g; Volume of $NaNO_3$ – 0.05 L; Concentration of $NaNO_3$ – 0.05; Time – 24 h (B) EGA dose – 0.1 g; Volume of NaCl – 0.05 L.

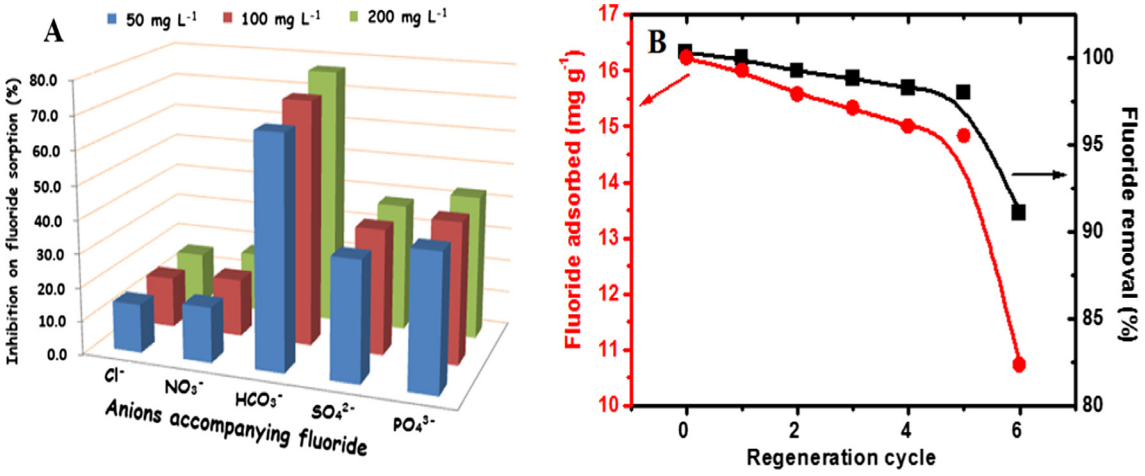

Fig. 8 Influence of co – ions during sorption of fluoride onto EGA_{NaCl} (A) and Regeneration of EGA_{NaCl} with first fluoride removal as reference (B). *Conditions:* (A) EGA dose – 0.1 g; Time – 35 min; T – 300 K (B) EGA dose – 0.1 g; Time – 35 min; T – 300 K; Regenerating solution – 0.05 M NaOH; V_{NaOH} – 0.05 L.

323 K, where about 1.95 fold (for the first two fluoride concentrations) was recorded against 1.27 fold between 3.41 mg L^{-1} and 5.31 mg L^{-1}. The direct proportionality of both temperature and fluoride concentration in driving the initial sorption rate (h) could be well established from the calculated data. An appreciable compliance of pseudo – second – order model than the pseudo – first – order model could be corroborated from the regression coefficient values (Table 1).

The following Eq. (13) for intra – particle diffusion determines the rate parameter for fluoride sorption onto EGA_{NaCl} (Mi et al., 2012).

$$q_t = k_{id}t^{1/2} + C_i \tag{13}$$

where k_{id} denotes the intra – particle diffusion rate constant (mg g^{-1} $min^{1/2}$) and C_i is the intercept defining the thickness of the boundary layer. The larger intercept value facilitates greater surface sorption and is the rate controlling step. When C_i becomes zero, intra – particle diffusion controls the rate of sorption throughout the sorption period with the observed linearity in the plot of q^t versus $t^{1/2}$. According to Allen et al. (1989), two portions of graphical curves could depict mesoporous and microporous diffusions. The straight line plots deviating from the origin attribute the difference in rates of mass transformation between initial and final adsorption stages (Mall et al., 2006). In the present fluoride sorption system, a multi-linear process is involved in the diffusion mechanism as shown in Fig. 9(D)–(F). The first, second and third sections of the curve correspond to the film diffusion (transport of fluoride from the bulk to the external surface of EGA_{NaCl}), intra – particle diffusion (diffusion from external surface into the pores of EGA_{NaCl}) and final equilibrium stage where the intra – particle diffusion starts to slow down. It can be understood from the non – zero C_i values that the intra – particle diffusion serves as a part and not the sole rate – determining in all the stages (Tang et al., 2012). In the fluoride sorption process, the initial film diffusion was then transformed as intra – particle diffusion and hence corroborated as the rate – controlling step. It may also be suggested that the average pore diameter (6.64 nm) could accommodate fluoride ions (ionic radius of 1.33 Å) during the movement of fluoride ions into the pores of EGA_{NaCl}. The regression coefficient values (Table 1) were recorded between 0.952 and 0.986 and approved

Table 1 Kinetic and isotherm data of fluoride sorption onto EGA_{NaCl}.

$[F]_o$	T = 300 K			T = 313 K			T = 323 K		
	2.78	3.41	5.31	2.78	3.41	5.31	2.78	3.41	5.31
Kinetic models									
1. Pseudo - first – order									
k_1	0.090	0.082	0.101	0.098	0.074	0.085	0.112	0.085	0.065
q_e	2.832	2.476	2.418	2.774	2.439	3.256	2.762	3.501	2.679
R^2	0.961	0.924	0.972	0.927	0.944	0.953	0.993	0.922	0.974
2. Pseudo - second – order									
k_2	0.003	0.009	0.016	0.006	0.009	0.005	0.009	0.003	0.008
q_e	23.256	25.641	55.556	24.391	31.251	66.667	27.027	52.632	66.667
h	1.621	6.329	50.001	3.425	9.346	20.833	6.412	6.849	33.333
R^2	0.987	0.991	0.999	0.989	0.993	0.996	0.999	0.984	0.997
3. Intra - particle diffusion									
k_i	2.816	1.953	1.735	2.552	2.073	4.382	2.362	5.501	2.881
C	0.431	11.892	13.372	5.714	16.703	35.104	10.78	17.783	44.053
R^2	0.983	0.971	0.963	0.964	0.968	0.986	0.952	0.984	0.981
4. Elovich									
A	2.174	8.891	15.912	54.619	169.847	18.879	353.117	333.586	262.91
B	0.186	0.205	0.218	0.272	0.258	0.097	0.302	0.121	0.184
R^2	0.983	0.963	0.989	0.943	0.929	0.957	0.963	0.964	0.958
Isotherm models									
1. Langmuir									
Q^o		4.863			12.883			16.267	
b		0.823			1.457			1.468	
R^2		0.995			0.997			0.995	
2. Freundlich									
n		4.047			5.231			7.299	
k_F		16.5			41.09			46.13	
R^2		0.899			0.876			0.859	
3. DKR									
E		12.9			15.8			22.37	
q_m		2.832			2.332			1.714	
R^2		0.998			0.990			0.995	

Units: k_1 – min^{-1}; k_2 – g mg^{-1} min^{-1}; k_i – mg g^{-1} $min^{-0.5}$; q and q_e – mg g^{-1}; h – mg g^{-1} min^{-1}; C – mg g^{-1}; A – mg g^{-1} min^{-1}; B – g mg^{-1}; Q^o – mg g^{-1}; b – L mg^{-1}; K_F – mg g^{-1}; q_m – mg g^{-1}; E – kJ mol^{-1}; n and R^2 – no unit.

the fit of intra – particle diffusion model. The agreeable fit and the direct proportionality between boundary layer effect and the initial fluoride concentration of this model are in agreement with the reported work of Li et al. (2016).

Elovich model (Aharoni and Tompkins, 1970) is one among the kinetic models to describe chemisorption and Eqs. (14) and (15) are as follows:

$$dq_t = Ae^{-Bqt} \tag{14}$$

The simplified form developed by Chien and Clayton (1980) is,

$$q_t = \left(\frac{1}{B}\right)\ln AB + \left(\frac{1}{B}\right)\ln t \tag{15}$$

where 'A' is the initial adsorption rate (mg g^{-1} min^{-1}) and 'B' is the constant of desorption (g mg^{-1}). The slope ($1/B$) obtained from the plot $\ln t$ versus q_t corresponds to the number of available sites for the accommodation of fluoride ions which could develop chemical forces (Juang and Chen, 1997). The initial adsorption rate was at its greater multiples at 313 K and 323 K than 300 K. The model plots are depicted in Fig. 9(G)–(I) and the validation can be ascertained from the R^2 values as shown in Table 1.

The adsorption isotherms express the specific relation between the concentration of adsorbate and its degree of accumulation onto adsorbent surface at a constant temperature. Based on the adsorption equilibrium data, three adsorption isotherm equations *viz.,* Langmuir isotherm, Freundlich isotherm and DKR were examined for understanding the thermodynamics of fluoride sorption onto EGA_{NaCl}. Based on the Langmuir isotherm (Langmuir, 1916), an adsorbent is assumed to have the monolayer adsorption on uniform homogeneous surface having identical sites without lateral interactions (Marani et al., 2016).

Langmuir Eqs. (16) and (17) are as follows:

$$Q_e = \frac{Q_o b C_e}{1 + bC_e} \tag{16}$$

$$\frac{C_e}{Q_e} = \frac{1}{Q^o b} + \frac{C_e}{Q^o} \tag{17}$$

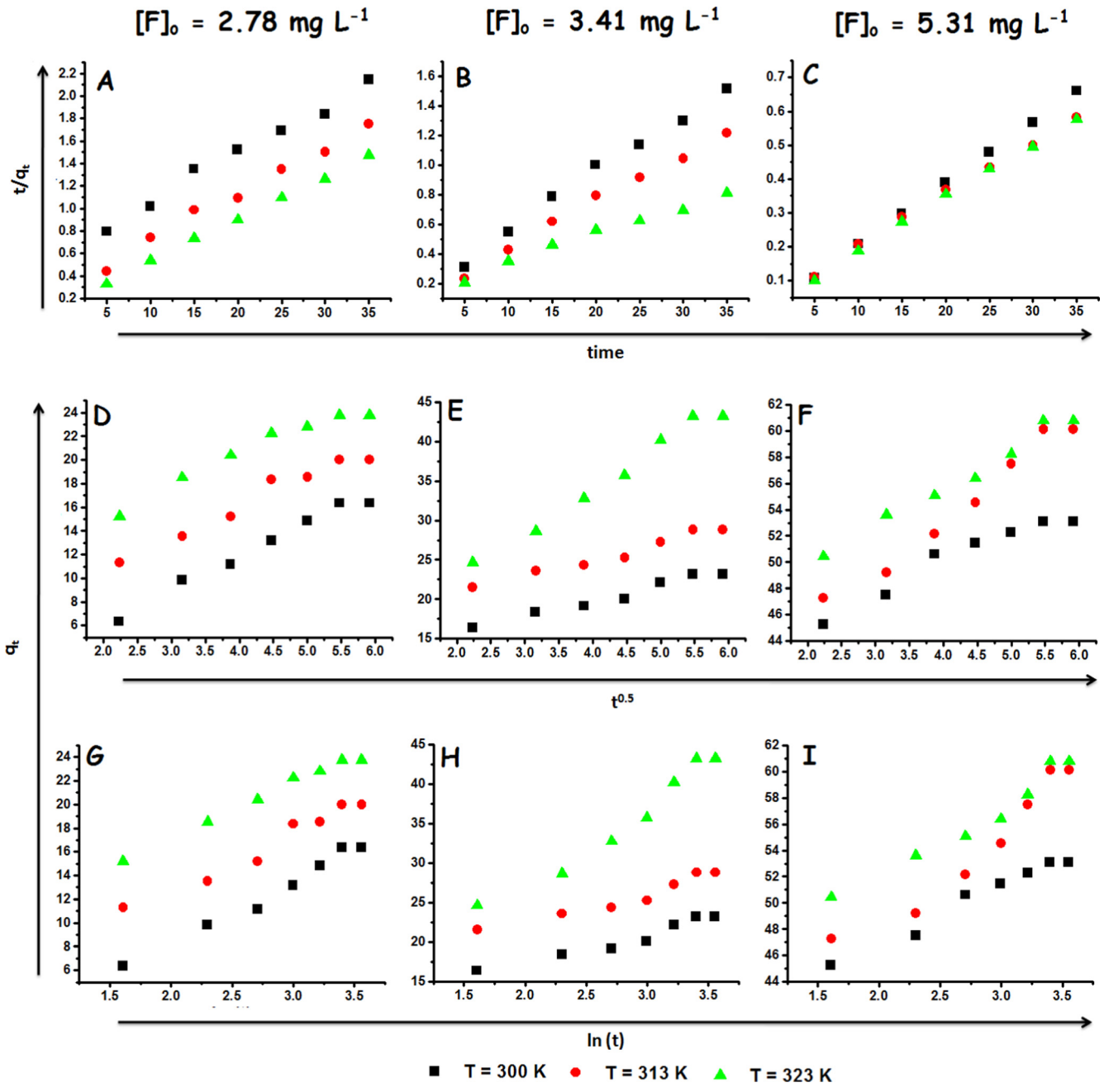

Fig. 9 Plots of kinetic models for different fluoride concentrations: Pseudo – second – order (A, B, C) Intra – particle – diffusion (D, E, F) Elovich (G, H, I); $[F]_0$ – Initial fluoride concentration.

The sorption capacity ($Q°$) is the amount of adsorbate at complete monolayer coverage (mg g^{-1}), C_e is the residual fluoride concentration at equilibrium (mg L^{-1}) and b (L mg^{-1}) is the Langmuir isotherm constant that relates the affinity of binding sites and the energy of adsorption. The respective values of $Q°$ and b were determined from the slope and the intercept of the straight line plot of C_e/q_e versus C_e (Table 1). The sorption capacity ($Q°$) increased from 4.683 mg g^{-1} to 16.267 mg g^{-1} on increasing the temperature from 300 K to 323 K (Fig. 10A). For the increase of 1.78 times in 'b', the sorption capacity was 3.34 times at 323 K. The influence of temperature on the sorption capacity confirmed the endothermic nature of sorption of fluoride onto EGA_{NaCl}. The regression values greater than 0.995 approved the excellent validation of the Langmuir model by suggesting the fluoride sorption on a homogeneous surface and preferably a monolayer. This observation is in agreement with the fluoride sorption onto mesoporous alumina, studied by Xu et al. (2016). The equilibrium saturation point characterized by the plateau of Langmuir model assumes the monolayer sorption on the sites without further sorption. In addition, Langmuir theory made an inverse relation between the distance and intermolec-

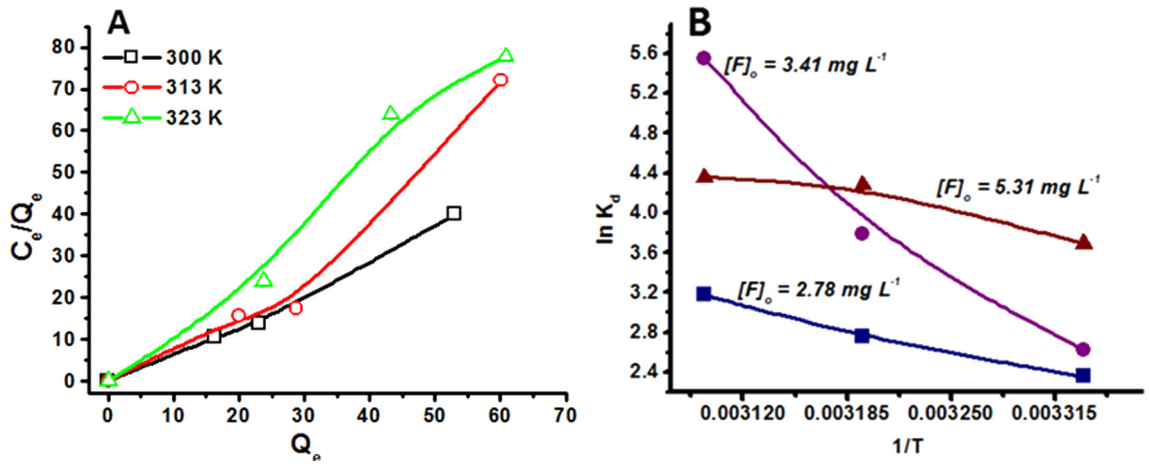

Fig. 10 Langmuir model (A) Plot of ln K_d versus $1/T$ (B).

ular attraction among molecules. Thus, another parameter R_L, a dimensionless constant separation factor (Weber and Chakravorti, 1974) can be calculated with the following Eq. (18),

$$R_L = 1\frac{1}{1+bC_o} \tag{18}$$

where 'C_o' is the initial fluoride concentration in mg L^{-1}. This parameter for the initial fluoride concentrations was calculated from 0.304 to 0.186 at 300 K, 0.194 to 0.111 at 313 K and 0.197 to 0.114 at 323 K. The value of R_L indicates the type of Langmuir isotherm as irreversible ($R_L = 0$), favorable ($0 < R_L < 1$), linear ($R_L = 1$) and unfavorable ($R_L > 1$). From the values obtained for the present fluoride sorption system, it is quite evident that the adsorption is favorable ($R_L < 1$) for the fluoride concentrations at all the temperatures.

Based on the Freundlich model (Freundlich, 1906) dealing with the multilayer sorption on a heterogeneous surface, Eq. (19) where, the Freundlich constants K_F (intercept) and n (as $1/n$ from the slope) are measures of adsorption capacity (mg g^{-1}) and adsorption intensity (or surface heterogeneity) respectively. The magnitude of $1/n$ is referred as a joint measure of both the relative magnitude and the diversities of energies associated with a particular sorption process (Karickhoff, 1981; Weber et al., 1992).

$$Q_e = K_F C_{e^{1/n}} \tag{19}$$

Evidently, from the decreased values of $1/n$ from 0.247 to 0.137, it is inferred that the surface heterogeneity is directly proportional to the temperature. In addition, the values of $1/n$ between 0 and 1 confirm the favorable conditions for the sorption of fluoride onto EGA.

On the other hand, the value of $n > 1$ at all the temperatures indicates the strong affinity between EGA and fluoride. The obtained linearity for the plot $\ln q_e$ versus $\ln C_e$ based on the regression values implies that the compliance of Freundlich model ($R^2 \geq 0.86$) is less than the Langmuir model and is represented in Table 1.

In order to comprehend the nature of adsorption, equilibrium data were tested with Dubinin–Radushkevich (DR) isotherm. The linearized DR equation is represented by Eq. (20) (Dubinin, 1960)

$$\ln q_e = \ln q_m - K\in^2 \tag{20}$$

where ε is Polanyi potential, and is equal to RT ln $(1 + 1/C_e)$, q_m is the theoretical adsorption capacity, K is the constant related to adsorption energy, R is universal gas constant (8.314 J mol^{-1} K^{-1}) and T is the temperature in Kelvin. DR isotherm constants K and q_m were calculated from the slope and intercept of the plot, respectively. The mean free energy of adsorption (E) was calculated from the constant K using Eq. (21)

$$E = (2K)^{-1/2} \tag{21}$$

E is defined as the free energy change for the transfer of one mole of ion from the surface of solid from infinity in solution. The increased mean free energy of adsorption was determined to be 12.9 kJ mol^{-1}, 15.8 kJ mol^{-1} and 22.37 kJ mol^{-1} respectively at 300 K, 313 K and 323 K as evidenced by early researchers (Gong et al., 2012). On the consideration of these values, it may be inferred that the present mechanism of fluoride sorption onto EGA_{NaCl} is governed by chemical forces. Thus DR model fits well with this fluoride sorption system as supported by the regression values ($R^2 \geq 0.99$). The validation of both Langmuir and DR models seems very good and hence the domination of chemical forces is mostly concerned between fluoride and EGA_{NaCl}.

3.5. Evaluation of thermodynamic parameters

The significance of thermodynamic analysis such as ΔH, ΔS and ΔG lies in its illustration of sorption mechanism and to study the nature of the process whether spontaneous or non-spontaneous and endothermic or exothermic. This parametric analysis is based on the calculation of temperature – dependent adsorption isotherms. The calculation of standard free energy change is possible from Eqs. (22) and (23),

$$\ln k_d = \frac{\Delta S_o}{R} - \frac{\Delta H_o}{RT} \tag{22}$$

$$\Delta G_o = -RT\ln k_d \tag{23}$$

where k_d is the distribution coefficient and its values can be obtained by plotting ln (q_e/C_e) versus C_e at different temperatures and extrapolating C_e to zero (Khan and Singh, 1987).

Table 2 Determination of thermodynamic parameters for fluoride sorption onto $EGA_{NaCl.}$

$[F]_o$	ΔH	ΔS	ΔG			
			300 K	313 K	323 K	E_a
2.78	28.376	0.114	−5.794	−7.306	−8.446	36.68
3.41	100.649	0.356	−6.152	−10.779	−14.339	37.57
5.31	24.135	0.109	−8.589	−9.985	−11.075	26.50

Except $[F]_o$ (mg L^{-1}) and ΔS^o (kJ mol^{-1} K^{-1}) all the other parameters (ΔG^o, ΔH^o and E_a) are expressed in kJ mol^{-1}.

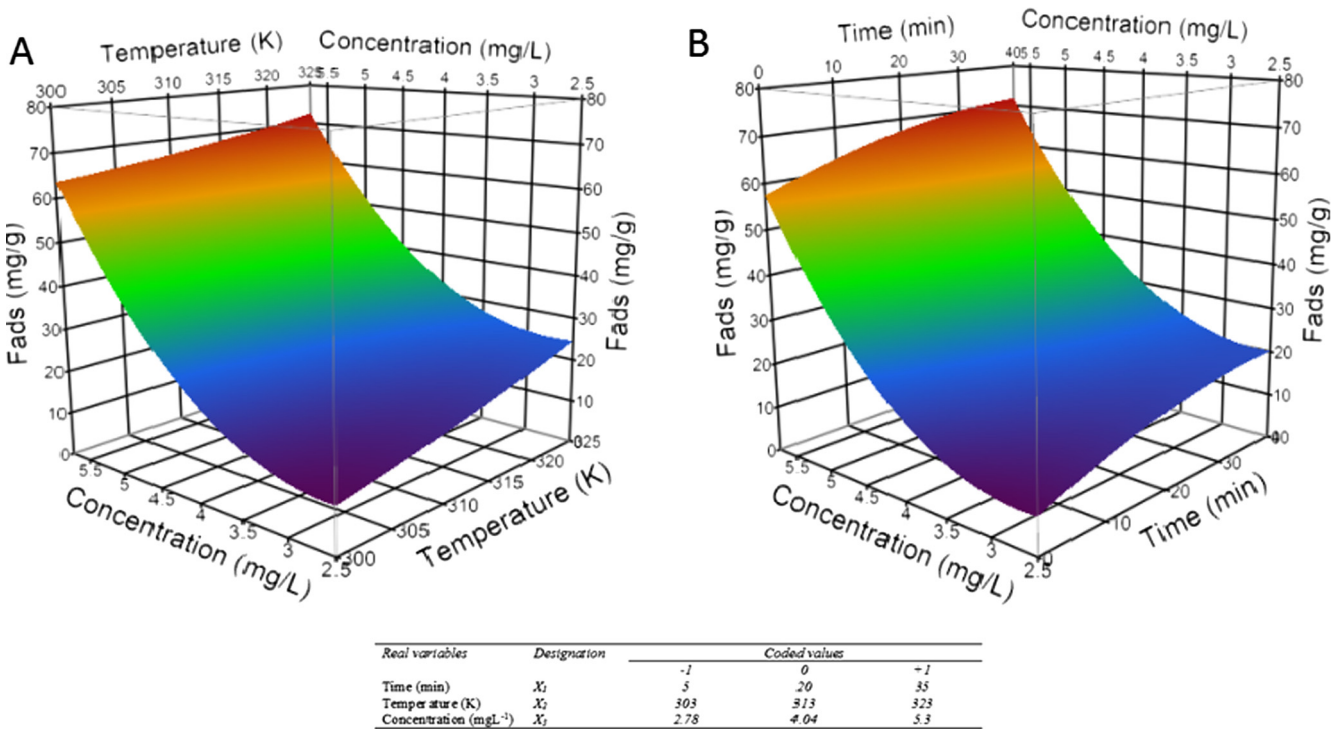

Fig. 11 The combined effect of temperature and fluoride concentration (A) time and fluoride concentration (B) on the adsorption of fluoride at pH 6.55 and EGA dose of 0.075 g.

The thermodynamic parameters are shown in Table 2. The negative ΔG values tend to increase with the increase in temperature and substantiate the feasibility of fluoride sorption onto $EGA_{NaCl.}$ The positive values of ΔH indicated the endothermic nature of fluoride sorption. The tendency of endothermic nature was increased from 2.78 mg L^{-1} to 3.41 mg L^{-1} but decreased thereafter. It corroborates the decreasing tendency of endothermic nature while increasing the concentration from 3.41 mg L^{-1} to 5.41 mg L^{-1}. The values of ΔH^o greater than 25 kJ mol^{-1} were inferred to be governed by chemical forces during the fluoride sorption (Gopal and Elango, 2007).

Likewise, the increased ΔS values indicated the increased randomness (at the solid/solution interface) of about 3.12 times from 2.78 mg L^{-1} to 3.41 mg L^{-1}. This may be due to the displacement of water molecules by fluoride species which leads to gain more translational entropy so as to allow the prevalence of randomness in the system (Doula et al., 2000). Conversely, the translational entropy loss at higher concentration of 5.41 mg L^{-1} may be the pertinent reason for the decrease in ΔS value.

The Arrhenius Eq. (24) is helpful to understand the nature of sorption based on physical forces with E_a value no more than 4.2 kJ mol^{-1} or chemical forces with E_a values between 8.4 kJ mol^{-1} and 83.7 kJ mol^{-1} (Aksu, 2002).

$$\ln k_d = \ln A_o - \left(\frac{E_a}{RT}\right) \tag{24}$$

where A_o is the temperature independent factor or frequency factor and E_a is the activation energy expressed in kJ mol^{-1} obtained from the plot as shown in Fig. 10B. The calculated E_a values of 36.68 kJ mol^{-1}, 37.57 kJ mol^{-1} and 26.50 kJ mol^{-1} respectively for 2.78 mg L^{-1}, 3.41 mg L^{-1} and 5.31 mg L^{-1} revealed the absolute dominance of chemical forces in the sorption of fluoride onto EGA_{NaCl}.

3.6. JMP statistical analysis

The present FFD system on the sorption of fluoride onto EGA_{NaCl} is applied to explore the effect of variables in the sorption process. FFD was applied to develop correlation between the variables operating aqueous fluoride solution

Table 3 Physical – structural characteristics of EGA_{NaCl}.

Parameter	Value
BET Surface area ($m^2\ g^{-1}$)	114.31
Langmuir Surface area ($m^2\ g^{-1}$)	283.41
External surface area ($m^2\ g^{-1}$)	117.35
Micropores surface area ($m^2\ g^{-1}$)	2.19
Cumulative surface area of pores, A ($m^2\ g^{-1}$)	121.88
Total pore volume, V_t ($cm^3\ g^{-1}$)	26.45
Micropore volume, V_m ($cm^3\ g^{-1}$)	0.0028
Porous volume of the monolayer ($cm^3\ g^{-1}$)	26.26
Cumulative volume of pores, V ($cm^3\ g^{-1}$)	0.2025
Average pore diameter, D (nm)	6.64

and the EGA_{NaCl}. The details about the range and levels of independent variables are given in the inserted table of Fig. 11. Two models were selected and applied using JMP statistical software version 10.0.0 (SAS Institute Inc., Cary, NC, USA).

The performance of regression analysis in fitting the response function of fluoride sorption ($mg\ g^{-1}$) was done. FED corroborates the influence of each factor on response and the interdependency among factors. The significant factors which affect the sorption of fluoride were determined by the performance of ANOVA. The variables denoted with coded values represent the sorption of fluoride as a function of time (X_1), temperature (X_2) and initial fluoride concentration (X_3). The final empirical models such as linear and quadratic models (as expressed by Eqs. (3) and (4)) in terms of coded factors for fluoride sorption are shown by Eqs. (25) and (26) respectively.

$$Y = 32.013 + 5.052X_1 + 4.737X_2 + 18.477X_3 + 1.239X_1X_2 + 0.306X_1X_3 - 0.799X_2X_3 \quad (25)$$

$$Y = -182.232 + 0.336X_1 + 0.474X_2 + 14.664X_3 + 0.006x_{1^2} + 0.005x_{2^2} + 5.209x_{3^2} + 0.008X_1X_2 + 0.016X_1X_3 - 0.063X_2X_3 \quad (26)$$

In Table 4 is represented the design of experiment with the observed and predicted removal of fluoride for quadratic and linear models. The observed values are the measured response data for a particular run whereas the predicted are based on model evaluation with the use of approximating functions. The variance of original observations is constant for all values of the response as inferred through the random scatter plot between Studentized residuals and predicted fluoride sorption.

The data analysis of variance (ANOVA) for the factorial design is summarized in Table 5. The values obtained as "Prob > F" less than 0.05 indicate that the terms are termed statistically significant. The factors such as time (X_1), temperature (X_2), fluoride concentration (X_3) and the squared interaction of fluoride concentration (X_3^2) are statistically significant at the 95% confidence level in the case of quadratic model. The coefficient of determination (R^2) of linear and quadratic model was 0.929 and 0.984 respectively and indicated an appreciable fit between predicted values and experimental data points. It can be corroborated that 92.9% (linear model) and

Table 4 Factorial design matrix with experimental and predicted responses.

Run	Independent variables			Linear model		Quadratic model	
	X_1	X_2	X_3	Observed	Predicted	Observed	Predicted
1	−	−	−	6.301	4.493	6.301	6.929
2	0	−	−	13.159	8.001	13.159	11.918
3	+	−	−	16.333	11.506	16.333	13.941
4	−	0	−	11.305	8.79	11.305	10.707
5	0	0	−	18.348	13.536	18.348	16.937
6	+	0	−	20.000	18.283	20.000	20.200
7	−	+	−	15.197	13.087	15.197	15.522
8	0	+	−	22.24	19.073	22.24	22.991
9	+	+	−	23.76	25.059	23.76	27.494
10	−	−	0	16.317	23.464	16.317	17.628
11	0	−	0	20.024	27.276	20.024	22.924
12	+	−	0	23.127	31.089	23.127	25.253
13	−	0	0	21.517	26.961	21.517	20.607
14	0	0	0	25.224	32.013	25.224	27.144
15	+	0	0	28.771	37.066	28.771	30.712
16	−	+	0	24.604	30.458	24.604	24.622
17	0	+	0	35.685	36.75	35.685	32.398
18	+	+	0	43.231	43.042	43.231	37.207
19	−	−	+	47.263	42.434	47.263	44.869
20	0	−	+	51.453	46.553	51.453	50.471
21	+	−	+	53.067	50.672	53.067	53.107
22	−	0	+	45.253	45.132	45.253	47.049
23	0	0	+	54.52	50.49	54.52	53.891
24	+	0	+	60.08	55.849	60.08	57.766
25	−	+	+	50.443	47.829	50.443	50.264
26	0	+	+	56.373	54.428	56.373	58.346
27	+	+	+	60.776	61.026	60.776	63.461

Table 5 Analysis of variance (ANOVA) for response surface quadratic and linear models for the fluoride sorption.

Source	Coefficient estimation		SS		DF		*F* value		Prob > *F*		Status	
	QM	LM	QM	LM	QM	LM	QM	LM	QM	LM	QM	LM
X_1	0.336	5.052	459.499	459.499	1	1	64.300	16.809	0.0006	<0.0001	Significant	Significant
X_2	0.473	4.737	403.895	403.895	1	1	56.519	14.775	0.001	<0.0001	Significant	Significant
X_3	14.664	18.477	6145.154	6145.154	1	1	859.922	224.801	<0.0001	<0.0001	Significant	Significant
X_1X_2	0.008	1.239	18.443	18.443	1	1	2.581	0.675	0.421	0.126		
X_1X_3	0.016	0.306	1.125	1.125	1	1	0.157	0.047	0.841	0.696		
X_2X_3	−0.063	−0.799	7.672	7.672	1	1	1.073	0.281	0.602	0.314		
X_1X_1	−0.006	NA	13.208	7035.79	1	NA	1.848	NA	NA	0.191		
X_2X_2	0.005	NA	1.607	546.719	1	NA	0.225	NA	NA	0.641		
X_3X_3	5.209	NA	410.418	7582.509	1	NA	57.432	NA	NA	<0.0001	Significant	
Model			7461.024		9	6	116.006	677.525				
Residual			121.485		17	20						
Total			7582.509		26	26			<0.0001	<0.0001	Significant	Significant
R^2	0.984	0.929										
R^2 adjusted	0.975	0.906										
RSD	32.014	32.014										
MR	32.013	34.376										

SS – Sum of squares; DF – Degree of freedom; Prob – Probability; QM – Quadratic Model; LM – Linear Model; RSD – Residual Standard Deviation; MR – Mean Response; X_1 – time; X_2 – temperature; X_3 – Initial fluoride concentration.

98.4% (quadratic model) of variation in the fluoride sorption are explained by the independent variables. The difference of R^2 and R^2_{adj} within ~0.2 is considered with reasonable agreement. In view of our case, the differences in R^2 and R^2_{adj} values obtained for linear and quadratic models are 0.023 and 0.009 respectively. However, these values are higher for quadratic model (0.984 & 0.975) than the linear model (0.929 & 0.906). Hence the validation of quadratic model with the fluoride sorption onto EGA_{NaCl} fits well to that of the linear model. It was justified that the insignificant terms interfere in the fair correlation coefficients and are likely the variable range with limited number of experiments and the nonlinear influence of parameters on the process response (Cronje et al., 2011; Sahu et al., 2009).

The investigation on the influencing three factors on fluoride sorption is depicted using the response surface methodology 3D plots (Fig. 11A and B). The combined effect of fluoride concentration and time at an optimized dose of 0.075 g and pH of 6.55 illustrates an initial raise of fluoride sorption in a gradual manner which later appeared to have a steep raise. The increase in fluoride sorption reaches the maximum value of greater than 70 mg g^{-1}. Similarly, the effect of fluoride concentration and temperature at an optimized pH and EGA_{NaCl} dose demonstrated the possible increase in fluoride sorption both with respect to initial concentration and temperature and hence the plots appear almost identical. But the steep raise in fluoride sorption for time – fluoride interaction is greater than that for concentration – temperature interaction. Hence it may be inferred that the influence of fluoride concentration is more predominate than the temperature. The plot for the combined effect of time and temperature for the fluoride concentration of 2.78 mg L^{-1} at an optimized pH and dose shows the gradual raise of fluoride sorption with the increase in temperature. However, the pattern shows the raise of fluoride sorption at lower temperature is gradual than the one at higher temperature appearing to have a steep pattern. Based on the mathematical equations developed for linear and quadratic models, the optimized fluoride sorption (at pH 6.55 and EGA_{NaCl} dose of 0.075 g) conditions according to linear model are 313 K and 5.31 mg L^{-1} (initial fluoride concentration), and according to quadratic model are 303 K and 5.31 mg L^{-1} of initial fluoride concentration. Nevertheless, the above optimal conditions for the fluoride sorption of 53.07 mg g^{-1} (predicted value is 53.11 mg g^{-1}) for the quadratic model and 45.25 mg g^{-1} (predicted value is 45.13 mg g^{-1}) for the linear model were observed. The lower temperature and higher fluoride sorption (at the same optimized dose and pH) seems suitable as per the conformity of quadratic model.

3.7. Regeneration of spent EGA_{NaCl}

An efficient regeneration process includes the factors such as, a remarkable removal, avoidance of excess regenerating solution and appreciable number of cycle operations. In our study, after optimizing the required sodium hydroxide of 0.05 M, the cycle of operation was admirable up to 5 times. The recorded removal efficiency was 99.3%, 97.9%, 97.1%, 96.1% and 95.5% for the first, second, third, fourth and fifth regenerations respectively (Fig. 8B). The difference in the removal percentage between first and fifth regeneration is about 3.8%. But on proceeding to sixth regeneration, the removal efficiency was dropped to 82.4% with a difference of 13.1%. Even though the following regenerations stand interrogative for further substantive efficiency, the retention more than 80% of removal after sixth regeneration is quite appealing. Although the regeneration was consistent in the beginning up to five cycles, the continuous interaction under basic condition during the sixth regeneration process could be the reason for initiating the dissolution of EGA_{NaCl}. Liu et al. (2011) studied the soluble Al species as $Al(OH)_4^-$ ions under basic conditions at pH > 9 using *in – situ* $Al_2O_3{\cdot}xH_2O$. The regeneration study attempted by Du and coworkers (Du et al., 2016) using 1×10^{-4} M NaOH was justifiable up to 2 cycles due to the Al loss from aluminum hydr(oxide) amended molecular sieves. Similar observation was reported using ordered mesoporous alumina (OMA 850) which could sustain the removal efficiency of about 80% after three cycles of operations (Ayoob and Gupta, 2009).

Table 6 Other alumina adsorbents for comparison with EGA_{NaCl}.

Adsorbent	Equilibrium time (min)	Q^o (mg g^{-1})	Reference
Magnetite – Al	1440	1.42	Garcia-Sanchez et al. (2016)
Activated aluminium-coated basalt fiber mat	240	1.84	Zhou et al. (2016)
Alkoxide origin alumina	1440	2.00	Kamble et al. (2010)
Nanoscale aluminium oxide hydroxide	360	4.90	Du et al. (2016)
PURAL® MG-20	1440	5.62	Patankar et al. (2013)
Alumina – modified expanded graphite composite	150	5.75	Jin et al. (2015)
Mesoporous alumina	180	8.25	Du et al. (2014)
Alumina cement granules	180	10.21	Ayoob and Gupta (2009)
Electro-coagulated metal hydroxide sludge	1440	11.32	Reyes Bahena et al. (2002)
MA	720	14.39	Garcia-Gomez et al. (2016)
Nano alumina	1500	15.43	Kumar et al. (2011)
EGA_{NaCl}	**35**	**16.33**	**Present study**
Porous alumina hollow spheres	400	16.77	Zhang and Jia (2016)
Aluminate impregnated alginate beads	480	17.00	Basu et al. (2013)
Mesoporous Al_2O_3	480	24.25	Dayananda et al. (2014)
Alum impregnated activated alumina	180	40.68	Tripathy et al. (2006)
Bayerite/boehmite nano composite	1440	56.80	Jia et al. (2015)
Amorphous aluminum hydroxide	10	63.94	Zhang and Jia (2016)
γ-AlOOH@CS magnetic nanoparticle	90	67.5	Wan et al. (2015)
Alumina (A2)	1400	89.29	Gong et al. (2012)
Ordered mesoporous alumina 400	3600	135.00	Yang et al. (2014)

3.8. Comparison with other aluminum adsorbents

Since EGA_{NaCl} is obtained from electrolysis with aluminum electrodes and its defluoridation efficiency can be compared to other defluoridation adsorbents containing aluminum. It can also be compared with electrocoagulation using aluminum electrodes.

Concerning the comparison, many papers give a table with adsorption capacities in the range 0.85–16.2 mg g^{-1} (Jin et al., 2015) or 0.37–8.40 mg g^{-1} (Goswami and Purkait, 2012). Some aluminum compounds show a greater adsorption capacity like 110 mg g^{-1} for freshly prepared aluminum hydroxides (Liu et al., 2011), or 62.5 mg g^{-1} for nanoscale aluminum hydroxide (Adeno et al., 2014) and 56.8 mg g^{-1} for bayerite/boehmite nanocomposites (Jia et al., 2015). A good comparison of defluoridation (Table 6) adsorbents needs more consideration than the adsorption capacity. Important results such as the equilibrium time and the efficiency of the regeneration of spent adsorbents must be taken into account. From this point of view, EGA_{NaCl} is an interesting and efficient adsorbent.

The comparison of a defluoridation adsorbent with an electrocoagulation is rarely discussed in the papers. With the results of the pioneering work of Ming et al. (1987), and assuming the formation of $Al(OH)_3$, it is possible to calculate a fluoride removal capacity of 30.46 mg g^{-1}. After five regeneration experiments (Fig. 8B) EGA_{NaCl} showed a fluoride removal capacity of 95.68 mg g^{-1} which correspond to a ratio Al/F of 2.8 instead of the ratio of 8 given by Ming et al. (1987). The chemical regeneration of EGA_{NaCl} which is an electrogenerated compound allows a more efficient defluoridation treatment than electrocoagulation.

4. Conclusion

The slow crystallization which occurred during the electrolysis at room temperature led to four crystallized aluminum compounds such as boehmite, bayerite, gibbsite and nordstrandite in EGA_{NaCl}. Despite its mixture composition, this material presented a good efficiency in the removal of fluoride from aqueous solution. Like aluminum hydroxides, EGA_{NaCl} showed a maximum of fluoride removal of 16.33 mg g^{-1} at pH 6.55. The equilibrium data were tested to fit Langmuir, Freundlich and DR isotherms in order to understand the mechanism of fluoride adsorption onto EGA_{NaCl}. The Langmuir isotherm model gave the best fit with the experimental data with the maximum adsorption capacity of EGA_{NaCl} of 16.27 mg g^{-1}. The free energy of adsorption at 27 °C was 12.9 kJ mol^{-1} which indicated the governance of chemical forces during sorption. The appreciable compliance of pseudo-second- order over other models was evaluated. The interference of hydrogen carbonate was high as compared to the other ions studied. Although the defluoridation capacity is fairly normal for EGA_{NaCl}, the regeneration study of the spent adsorbent using 0.05 M NaOH allowed up to 95.5% of defluoridation efficiency during the first cycle. The total performance of the spent EGA_{NaCl} was superior to that of a published electrocoagulation process. Hence, the successive regenerations of EGA_{NaCl} could enable to minimize the waste production when it is compared to electrocoagulation. The response surface methodology revealed the superiority of quadratic model over linear model and suggested the suitability of defluoridation process at 303 K and 5.31 mg L^{-1} of initial fluoride concentration.

Acknowledgments

We would like to thank the heads of the collaborating institutes, namely CNRS, National College of Chemistry (ENSCR, Rennes, France), P. G. and Research Department of Chemistry of Pachaiyappa's College (Chennai, India), Nagasaki University (Japan), University of South Africa (Johannesburg, South Africa) and University of Sciences and Technology Houari Boumédiène (Algiers, Algeria). The corresponding author (V. Sivasankar) thanks JSPS for having awarded him the JSPS overseas fellowship for the year 2016. Loïc Joanny is acknowledged for EDS analyses performed at CMEBA (ScanMat, University of Rennes-1) which received a financial support from the Région Bretagne and European Union (CPER-FEDER 2007-2014).

References

Adeno, F., Mulugeta, E., Zewge, F., Chebude, Y., 2014. Adsorptive removal of fluoride from water using nanoscale aluminium oxide hydroxide (AlOOH). Bull. Chem. Soc. Ethiop. 28, 215–227.

Aharoni, C., Tompkins, F.C., 1970. Kinetics of Adsorption and Desorption and the Elovich Equation. Advance in Catalysis and related subjects. Academic Press, New York.

Aksu, A., 2002. Determination of the equilibrium, kinetic and thermodynamic parameters of the batch biosorption of nickel(II) ions onto Chlorella vulgaris. Process Biochem. 38, 89–99.

Alam, M.Z., Muyibi, S.A., Toramae, J., 2007. Statistical optimization of adsorption processes for removal of 2,4-dichlorophenol by activated carbon derived from oil palm empty fruit bunches. J. Environ. Sci. 19, 674–677.

Allen, S.J., McCay, G., Khader, K.Y.H., 1989. Intraparticle diffusion of a basic dye during adsorption onto sphagnum peat. Environ. Pollut. 56, 39–50.

Ayoob, S., Gupta, A.K., Bhakat, P.B., Bhat, V.T., 2008. Investigations on the kinetics and mechanisms of sorptive removal of fluoride from water using alumina cement granules. Chem. Eng. J. 140, 6–14.

Ayoob, S., Gupta, A.K., 2009. Performance evaluation of alumina cement granules in removing fluoride from natural and synthetic waters. Chem. Eng. J. 150, 485–491.

Basu, H., Singhal, R.K., Pimple, M.V., Reddy, A.V.R., 2013. Synthesis and characterization of alumina impregnated alginate beads for fluoride removal from potable water. Water, Air, Soil Pollut. 224, 1572–1584.

Benítez-Guerrero, M., Pérez-Maqueda, L.A., Sánchez-Jiménez, P.E., Pascual-Cosp, J., 2014. Characterization of thermally stable gamma alumina fibres biomimicking sisal. Microporous Mesoporous Mater. 185, 167–178.

Betiha, M.A., Mahmoud, S.A., Menoufy, M.F., Al-Sabagh, A.M., 2011. One pot template synthesis of Ti-Al- containing mesoporous silicas and their application as potential photocatalytic degradation of chlorophenols. Appl. Catal. B: Environ. 107, 316–326.

Box, G.E.P., Hunter, J.S., 1975. Multi-factor experimental design for exploring response surfaces. Ann. Math. Stat. 28, 195–241.

Chauhan, V.S., Dwivedi, P.D., Iyengar, L., 2007. Investigations on activated alumina based domestic defluoridation units. J. Hazard. Mater. B139, 103–107.

Chien, S.H., Clayton, W.R., 1980. Application of Elovich equation to the kinetics of phosphate release and sorption in soils. Soil Sci. Soc. Am. J. 44, 265–268.

Cronje, K.J., Chetty, K., Carsky, M., Sahu, J.N., Meikap, B.C., 2011. Optimization of chromium (VI) sorption potential using developed activated carbon from sugarcane bagasse with chemical activation by zinc chloride. Desalination 275, 276–284.

Darchen, A., Sivasankar, V., Chaabane, T., Prabhakaran, M., 2016. Methods of defluoridation: adsorption and regeneration of adsorbents. In: Sivasankar, V. (Ed.), Surface Modified Carbons as Scavengers for Fluoride from Water. Springer, pp. 63–92.

Dayananda, D., Sarva, V.R., Prasad, S.V., Arunachalam, J., Ghosh, N.N., 2014. Preparation of CaO loaded mesoporous Al_2O_3: Efficient adsorbent for fluoride removal from water. Chem. Eng. J. 248, 430–439.

Dubinin, M.M., 1960. The potential theory of adsorption gases and vapors for adsorbents with energetically non – uniform surfaces. Chem. Rev. 60, 235–241.

Doula, M., Ioannou, A., Dimirkou, A., 2000. Thermodynamics of copper adsorption–desorption by Ca-kaolinite. Adsorption 6, 325–335.

Du, J., Sabatini, D.A., Butler, E.C., 2014. Synthesis, characterization, and evaluation of simple aluminium – based adsorbents for fluoride removal from drinking water. Chemosphere 101, 21–24.

Du, J., ASCE, S.M., David, A., Sabatini, M., ASCE, M., Butler, E.C., 2016. Preparation, characterization, and regeneration of Aluminium hydr(oxide) – Amended molecular sieves for fluoride removal from Drinking water. J. Environ. Eng. 142 (10), 1–8. http://dx.doi.org/10.1061/(ASCE)EE.1943-7870.0001114.

Elderfield, H., Hem, J.D., 1973. The development of crystalline structure in aluminium hydroxide polymorphs on ageing. Mineral. Mag. 39, 89–96.

Fang, Z., Xue, N., Li, L., Hong, T., Kong, H., Wu, J., 2016. Performance and mechanism for defluoridation by modified aluminium hydroxide in zinc sulfate solution. J. Nanosci. Nanotechnol. 16 (12), 12470–12475.

Flilissa, A., Meleard, P., Darchen, A., 2016. Cetylpyridinium removal using phosphateassisted electrocoagulation, electroreduction and adsorption on electrogenerated sorbents. Chem. Eng. J. 284, 823–830.

Freundlich, H.M.F., 1906. Uber die adsorption in losungen. Z. Phys. Chem. 57A, 385–470.

Ganvir, V., Das, K., 2011. Removal of fluoride from drinking water using aluminum hydroxide coated rice hush ash. J. Hazard. Mater. 185, 1287–1294.

Garcia-Gomez, C., Rivera-Huerta, M.L., Almazan-Garcia, F., Martin-Dominguez, A., Romero-Soto, I.C., Burboa-Charis, V.A., Gortares-Moroyoqui, P., 2016. Electrocoagulated metal hydroxide sludge for fluoride and arsenic removal in aqueous solution: Characterization, kinetic and equilibrium studies. Water Air Soil Pollut. 227, 1–16. http://dx.doi.org/10.1007/s11270-016-2783-5.

Garcia-Sanchez, J.J., Solache-Rios, M., Martinez-Gutierrez, J.M., Arteaga-Larios, N.V., Ojeda-Escamilla, M.C., Rodriguez-Torres, I., 2016. Modified natural magnetite with Al and La ions for the adsorption of fluoride ions from aqueous solutions. J. Fluorine Chem. 186, 115–124.

George, S., Pandit, P., Gupta, A.B., 2010. Residual aluminium in water defluoridated using activated alumina adsorption – Modeling and simulation studies. Water Res. 44, 3055–3064.

Ghorai, S., Pant, K.K., 2004. Investigations on the column performance of fluoride adsorption by activated alumina in a fixed-bed. Chem. Eng. J. 98, 165–173.

Guzman, A., Nava, J.L., Coreno, O., Rodriguez, I., Gutierrez, S., 2016. Arsenic and fluoride removal from groundwater by electrocoagulation using a continuous filter-press reactor. Chemosphere 144, 2113–2120.

Golder, A.K., Samanta, A.N., Ray, S., 2006a. Removal of phosphate from aqueous solutions using calcined metal hydroxides sludge waste generated from electrocoagulation. Sep. Purif. Technol. 52, 102–109.

Golder, A.K., Samanta, A.N., Ray, S., 2006b. Anionic reactive dye removal from aqueous solution using a new adsorbent – Sludge generated in removal of heavy metal by electrocoagulation. Chem. Eng. J. 122, 107–115.

Gong, W.-X., Qu, J.-H., Liu, R.-P., Lan, H.-C., 2012. Adsorption of fluoride onto different types of aluminas. Chem. Eng. J. 189–190, 126–133.

Gopal, V., Elango, K.P., 2007. Equilibrium, kinetic and thermodynamic studies of adsorption of fluoride onto plaster of Paris. J. Hazard. Mater. 141, 98–105.

Goswami, A., Purkait, M.K., 2012. The defluoridation of water by acidic alumina. Chem. Eng. Res. Des. 90, 2316–2324.

Gunaraj, V., Murugan, N., 1999. Application of response surface methodologies for predicting weld base quality in submerged arc welding of pipes. J. Mater. Process. Technol. 88, 266–275.

Hao, J.O., Huang, C.P., 1986. Adsorption characteristics of fluoride onto hydrous alumina. J. Environ. Eng. (ASCE) 112, 1054–1067.

Ho, Y.S., 2006. Second-order-kinetic model for the sorption of cadmium onto tree fern: a comparison of linear and non-linear methods. Water Res. 40, 119–125.

Ho, Y.S., 2004. Citation review of Lagergren Kinetic rate equation on adsorption reactions. Scientometrics 59, 171–177.
Jia, Y., Zhu, B.-S., Jin, Z., Sun, B., Luo, T., Yu, X.-Y., Kong, L.-T., Liu, J.-H., 2015. Fluoride removal mechanism of bayerite/boehmite nanocomposites: roles of the surface hydroxyl groups and the nitrate anions. J. Colloid Interface Sci. 440, 60–67.
Jimenez-Becerril, J., Solache-Rios, M., Garcia-Sosa, I., 2012. Fluoride removal from aqueous solutions by Boehmite. Water Air Soil Pollut. 223, 1073–1078.
Jin, H.Y., Ji, Z.J., Yuan, J., Li, J., Liu, M., Xu, C.H., Dong, J., Hou, P., Hou, S., 2015. Research on removal of fluoride in aqueous solution by alumina-modified expanded graphite composite. J. Alloy. Compd. 620, 361–367.
Juang, R.S., Chen, M.L., 1997. Application of the Elovich equation to the kinetics of metal sorption with solvent-impregnated resins. Ind. Eng. Chem. Res. 36, 813–820.
Kamble, S.P., Deshpande, G., Barve, P.P., Rayalu, S., Labhsetwar, N. K., Malyshew, A., Kulkarni, B.D., 2010. Adsorption of fluoride from aqueous solution by alumina of alkoxide nature: Batch and continuous operation. Desalination 264, 15–23.
Karickhoff, S.W., 1981. Semi-empirical estimation of sorption of hydrophobic pollutants on natural sediments and soil. Chemosphere 10, 833–846.
Khan, A.A., Singh, R.P., 1987. Adsorption thermodynamics of carbofuran on Sn(IV) arsenosilicate in H+, Na+ and Ca2+ forms. Colloids Surf. 24, 33–42.
Killedar, D.J., Bhargava, D.S., 1993. Effect of stirring rate and temperature on fluoride removal by fishbone charcoal. Indian J. Environ. Health 35, 81–87.
Ku, Y., Chiou, H.M., 2002. The adsorption of fluoride ion from aqueous solution by activated alumina. Water Air Soil Pollut. 133, 349–360.
Kumar, E., Bhatnagar, A., Kumar, U., Sillanpää, M., 2011. Defluoridation from aqueous solutions by nano-alumina: characterization and sorption studies. J. Hazard. Mater. 186, 1042–1049.
Lagergren, S., 1898. Zur theorie der sogenannten adsorption geloster stoffe Kungliga Svenska Vetenskapsakademiens. Handligar 24, 1–39.
Langmuir, I., 1916. The constitution and fundamental properties of solids and liquids. J. Am. Chem. Soc. 38, 2221–2295.
Li, C., Chen, N., Zhao, Y., Li, R., Feng, C., 2016. Polypyrrole – grafted peanut shell biological carbon as a potential sorbent for fluoride removal: Sorption capability and mechanism. Chemosphere 163, 81–89.
Liu, R., Gong, W., Lan, H., Gao, Y., Liu, H., Qu, J., 2011. Defluoridation by freshly prepared aluminum hydroxides. Chem. Eng. J. 175, 144–149.
Mall, I.D., Srivastava, V.C., Kumar, G.V.A., Mishra, I.M., 2006. Characterization and utilization of mesoporous fertilizer plant waste carbon for adsorptive removal of dyes from aqueous solution. Colloids Surf. A 278, 175–187.
Maliyekkal, S.M., Shukla, S., Philip, L., Nambi, I.M., 2008. Enhanced fluoride removal from drinking water by magnesia-amended activated alumina granules. Chem. Eng. J. 140, 183–192.
Marani, D., Sudireddy, B.R., Nielsen, L., Ndoni, S., Kiebach, R., 2016. Poly(vinylpyrrolidone) as dispersing agent for cerium-gadolinium oxide (CGO) suspensions. J. Mater. Sci. 51, 1098–1106.
Mi, X., Huang, G., Xie, W., Wang, W., Liu, Y., Gao, J., 2012. Preparation of graphene oxide aerogel and its adsorption for Cu2+ ions. Carbon 50, 4856–4864.
Ming, L., Yi, S.R., Hua, Z.J., Yuan, B., Lei, W., Ping, L., Fuwa, K.C., 1987. Elimination of excess fluoride in potable water with coacervation by electrolysis using an aluminum anode. Fluoride 20, 54–63.
Montgomery, D.C., 2001. Design and Analysis of Experiments. John Wiley and Sons, New York, USA.
Music, S., Dragcevic, D., Popovic, S., Vdovic, N., 1998. Microstructural properties of boehmite formed under hydrothermal conditions. Mater. Sci. Eng., B 52, 145–153.
Murray, J.W., Stumm, W. (Eds.), 1988. Aquatic Surface Chemistry: Chemical Processes at the Particle-Water Interface, vol. 52. John Wiley & Sons, New York, p. 1742.
Netpradit, S., Thiravetyan, P., Towprayoon, S., 2004. Adsorption of three azo reactive dyes by metal hydroxide sludge: effect of temperature, pH, and electrolytes. J. Colloid Interface Sci. 270, 255–261.
Nigussie, W., Zewge, F., Chandravanshi, B.S., 2007. Removal of excess fluoride from water using waste residue from alum manufacturing process. J. Hazard. Mater. 147, 954–963.
Nordin, J.P., Sullivan, D.J., Phillips, B.L., Casey, W.H., 1999. Mechanisms for fluoride-promoted dissolution of bayerite [β-Al(OH)3(s)] and boehmite [γ-AlOOH]: ^{19}F-NMR spectroscopy and aqueous surface chemistry. Geochim. Cosmochim. Acta 63, 3513–3524.
Ogorodova, L.P., Kiseleva, I.A., Sokolova, E.L., Vigasina, M.F., Kabalov, Yu.K., 2012. Thermochemical study of polymorphic modifications of Al(OH)3: gibbsite and nordstrandite. Geochem. Int. 50, 90–94.
Patankar, G.V., Tambe, A.S., Kulkarni, B.D., Malyshew, A., Kamble, S.P., 2013. Defluoridation of drinking water using PURAL® MG-20 mixed hydroxide adsorbent. Water Air Soil Pollut. 224, 1727–1740.
Raichur, A.M., Basu, M.J., 2001. Adsorption of fluoride onto mixed rare earth oxides. Sep. Purif. Technol. 24, 121–127.
Reyes Bahena, J.L., Robledo Cabrera, A., López Valdivieso, A., Herrera Urbina, R., 2002. Fluoride adsorption onto α-Al_2O_3 and its effect on the zeta potential at the alumina–aqueous electrolyte interface. Sep. Sci. Technol. 37, 1973–1987.
Sahu, J.N., Acharya, J., Meikap, B.C., 2009. Response surface modeling and optimization of chromium (VI) removal from aqueous solution using Tamarind wood activated carbon in batch process. J. Hazard. Mater. 172, 818–825.
Saleh, T.A., Gupta, V.K., 2012. Synthesis and characterization of alumina nano-particles polyamide membrane with enhanced flux rejection performance. Sep. Purif. Technol. 89, 245–251.
Santos, S.C.R., Vilar, V.J.P., Boaventura, R.A.R., 2008. Waste metal hydroxide sludge as adsorbent for a reactive dye. J. Hazard. Mater. 153, 999–1008.
Schoeman, J.J., 2009. Performance of a water defluoridation plant in a rural area in South Africa. Water SA 2009 (35), 97–101.
Shimelis, B., Zewge, F., Chandravanshi, B.S., 2006. Removal of excess fluoride from water by aluminum hydroxide. Bull. Chem. Soc. Ethiop. 20, 17–34.
Wang, Shu-Guang, Ma, Y., Shi, Yi-Jing, Gong, Wen-Xin, 2009a. Defluoridation performance and mechanism of nano-scale aluminum oxide hydroxide in aqueous solution. J. Chem. Technol. Biotechnol. 84, 1043–1050.
Singh, I.B., Gupta, A., Dubey, S., Shafeeq, M., Banerjee, P., Sinha, A. S.K., 2016. Sol-gel synthesis of nanoparticles of gamma alumina and their application in defluoridation of water. J. Sol-Gel Technol. 77, 416–422.
Sivasankar, V., 2016. Surface Modified Carbons as Scavengers for Fluoride from Water. Springer.
Sing, K.S.W., Everett, D.H., Haul, R.A.W., Moscou, L., Pierotti, R. A., Rouquérol, J., Siemieniewska, T., 1985. Reporting Physisorption data for gas/solid systems with special reference to the determination of surface area and porosity. Pure Appl.Chem. 57, 603–619.
Sujana, M.G., Thakur, R.S., Rao, S.B., 1998. Removal of fluoride from aqueous solutions by using alum sludge. J. Colloid Interface Sci. 206, 94–101.

Tang, H., Zhou, W., Zhang, L., 2012. Adsorption isotherms and kinetic studies of malachite green on chitin hydrogels. J. Hazard. Mater. 209–210, 218–225.

Tangsir, S., Hafshejani, L.D., Lähde, A., Maljanen, M., Hooshmand, A., Naseri, A.A., Moazed, H., Jokiniemi, J., Bhatnagar, A., 2016. Water defluoridation using Al2O3 nanoparticles synthesized by flame spray pyrolysis (FSP) method. Chem. Eng. J. 288, 198–206.

Tchomgui-Kamga, E., Audebrand, N., Darchen, A., 2013. Effect of co-existing ions during the preparation of alumina by electrolysis with aluminum soluble electrodes: structure and defluoridation activity of electro-synthesized adsorbents. J. Hazard. Mater. 254–255, 125–133.

Teutli-Sequeira, A., Solache-Rios, M., Balderas-Hernandez, P., 2012. Modification effects of Hematite with aluminium hydroxide on the removal of fluoride ions from water. Water Air Soil Pollut. 223, 319–327.

Tripathy, S.S., Bersillon, J.-L., Gopal, K., 2006. Removal of fluoride from drinking water by adsorption onto alum-impregnated activated alumina. Sep. Purif. Technol. 50, 310–317.

US EPA, 2003. Water treatment technology feasibility support document for chemical contaminants. In: Support of EPA Six-Year Review of National Primary Drinking Water Regulations. EPA 815-R-03-004, 36 pages.

Wan, Z., Chen, W., Liu, Y., Liu, Y., Dong, C., 2015. Preparation and characterization of γ-AlOOH@CS magnetic nanoparticle as a novel adsorbent for removing fluoride from drinking water. J. Colloid Interface Sci. 443, 115–124.

Wang, S.-G., Ma, Y., Shi, Y.J., Gong, W.-X., 2009b. Defluoridation performance and mechanism of nano-scale aluminium oxide hydroxide in aqueous solution. J. Chem. Technol. Biotechnol. 84, 1043–1050.

Weber, T.W., Chakravorti, R.K., 1974. Pore and solid diffusion models for fixed-bed adsorbers. AlChE J. 1974 (20), 228–237.

Weber, W.J., McGinley, P.M., Katz, L.E., 1992. A distributed reactivity model for sorption by soils and sediments. 1. Conceptual basis and equilibrium assessments. Environ. Sci. Technol. 26, 1955–1962.

Wu, S., Zhang, K., He, J., Cai, X., Chen, K., Li, Y., Sun, B., Kong, L., Liu, J., 2016. High efficient removal of fluoride from aqueous solution by a novel hydroxyl aluminum oxalate adsorbent. J. Colloid Interface Sci. 464, 238–245.

Xu, N., Liu, Z., Dong, Y., Hong, T., Dang, L., Li, W., 2016. Controllable synthesis of mesoporous alumina with large surface area for high and fast fluoride removal. Ceram. Int. 42, 15253–15260.

Yang, C., Gao, L., Wang, Y., Tian, X., Komarneni, S., 2014. Fluoride removal by ordered and disordered mesoporous aluminas. Microporous Mesoporous Mater. 197, 156–163.

Zaidi, S., Chaabane, T., Sivasankar, V., Darchen, A., Maachi, R., Msagati, T.A.M., Prabhakaran, M., 2016. Performance efficiency of electro-coagulation coupled electroflotation process (EC-EF) versus adsorption process in doxycycline removal from aqueous solutions. Process Saf. Environ. Protect. 102, 450–461.

Zhang, Y.-X., Jia, Y., 2016. Fluoride adsorption onto amorphous aluminium hydroxide: Roles of the surface acetate ions. J. Colloid Interface Sci. 483, 295–306.

Zhou, Q., Liang, X., Wang, J., Wang, H., Chen, P., Zhang, D., Yang, S., Li, J., 2016. Preparation of activated aluminium-coated basalt fiber mat for defluoridation from drinking water. J. Sol-Gel Sci. Technol. 78, 331–338.

Zidane, F., Drogui, P., Lekhlif, B., Bensaid, J., Blais, J.-F., Belcadi, S., El Kacemi, K., 2008. Decolourization of dye-containing effluent using mineral coagulants produced by electrocoagulation. J. Hazard. Mater. 155, 153–163.

Zou, Y., Wang, X., Chen, Z., Yao, W., Ai, Y., Liu, Y., Hayat, T., Alsaedi, A., Alharbi, N.S., Wang, X., 2016. Superior coagulation of graphene oxides on nanoscale layered double hydroxides and layered double hydroxides. Environ. Pollut. 219, 107–117.